Geophysical and hydrogeological survey in a part of the Nhandugue River valley, Gorongosa National Park, Mozambique – Area 1 and 2

Li Stenberg

Mastern thesis in geology at Lund University - Quaternary Sciences, no. 266
(45 hskp/ECTS)

Minor Field Studies (MFS) Scholarship Programme

Department of Earth- and Ecosystem Sciences
Division of Geology
Lund University
2010

Geophysical and hydrogeological survey in a part of the Nhandugue River valley, Gorongosa National Park, Mozambique - Area 1 and 2

Master Thesis

Li Stenberg

Department of Earth and Ecosystem Sciences
Division of Geology
Lund University

2010

LUNDS TEKNISKA HÖGSKOLA
Lunds universitet

Lund University
Faculty of Engineering, LTH
Departments of Earth and Water Engineering

This study has been carried out within the framework of the Minor Field Studies (MFS) Scholarship Programme, which is funded by the Swedish International Development Cooperation Agency, Sida.

The MFS Scholarship Programme offers Swedish university students an opportunity to carry out two months' field work in a developing country resulting in a graduation thesis work, a Master's dissertation or a similar in-depth study. These studies are primarily conducted within subject areas that are important from an international development perspective and in a country supported by Swedish international development assistance.

The main purpose of the MFS Programme is to enhance Swedish university students' knowledge and understanding of developing countries and their problems. An MFS should provide the student with initial experience of conditions in such a country. A further purpose is to widen the human resource base for recruitment into international co-operation. Further information can be reached at the following internet address: http://www.tg.lth.se/mfs.

The responsibility for the accuracy of the information presented in this MFS report rests entirely with the authors and their supervisors.

Gerhard Barmen
Local MFS Programme Officer

Postadress Box 118, 221 00 Lund *Besöksadress* John Ericssons väg 1 *Telefon dir* 046-222 9657, *växel* 046-222 00 00 *Telefax* 046-2229127
E-post Gerhard.Barmen@tg.lth.se

Contents

Cover Picture: Nhandugue River, Gorongosa National Park, Mozambique. Photo: Li Stenberg

Contents

Geophysical and hydrogeological survey in a part of the Nhandugue River valley, Gorongosa National Park, Mozambique — Area 1 and 2.

LI STENBERG

Stenberg, L., 2010: Geophysical and hydrogeological survey in a part of the Nhandugue River valley, Gorongosa National Park, Mozambique — Area 1 and 2. *Examensarbeten i geologi vid Lunds universitet*, Nr. 266, 46 pp. 45 hp.

Abstract: Gorongosa National Park in central Mozambique is situated at the southernmost extension of the East African Rift System (EARS), the Urema Graben. The Nhandugue River flows over the western margin of the Urema Graben, and marks the northwest border of Gorongosa National Park, Mozambique. The park is protecting a vast ecosystem of floodplains, grasslands and woody coverage.

The study is focused on the western rift margin, using resistivity measurements, shallow auger drilling for soil sampling, and discharge measurements to give more information about the hydrological conditions.

The resistivity results suggest that the area is heavily faulted and most likely constitutes a major groundwater recharge zone. Moving from the rift margin and into the rift valley, the resistivity models indicate that solid gneiss is replaced by fractured and weathered gneiss, sandstone and alluvial sediments. The top 10-15 m of this sequence measure high resistivity, interpreted as alluvial sand. It extends back to the rift margin thus also covering the gneiss. The sandstone outcrops a few kilometers from the rift margin and dips towards the southeast. Further into the rift valley, the alluvial sand is underlain by low resistivity lenses of silt/clay, followed by a medium resistivity layer of sand.

The topmost layer of alluvial sand constitutes an unconfined aquifer under which the solid gneiss forms a hydraulic boundary. The adjacent fractured gneiss, however, has been interpreted as an unconfined fractured aquifer and a zone of infiltration. The sandstone is also considered to be unconfined, while the lenses of silt/clay constitutes an aquiclude, underlain by the sand, and representing a semi-confined aquifer.

The discharge measurements show a large downstream decrease in runoff, suggesting that the surface water is infiltrating and recharging the aquifers, and is then transported as ground water in a southeast direction.

Keywords: Mozambique, Geophysical investigation, Gorongosa National Park, Groundwater recharge zone, Nhandugue River, Urema Graben.

Li Stenberg, Institutionen för geo– och ekosystemvetenskaper, enheten för geologi, Centrum för GeoBiosfärsvetenskap, Lunds Universitet, Sölvegatan 12, 223 62 Lund, Sverige. E-post: li.stenberg@hotmail.com

Geofysisk och hydrogeologisk undersökning i en del av Nhandugueflodens floddal, Gorongosa Nationalpark, Moçambique — Område 1 och 2.

LI STENBERG

Stenberg, L., 2010: Geofysisk och hydrogeologisk undersökning i en del av Nhandugueflodens floddal, Gorongosa Nationalpark, Moçambique — Område 1 och 2. *Examensarbeten i geologi vid Lunds universitet*, Nr. 266, 46 sid. 45 hp.

Sammanfattning: Gorongosa Nationalpark i centrala Mozambiqe ligger i den sydligaste delen av det Östafrikanska riftsystemet Urema Graben. Nhandugue floden flyter över kanten av den västra marginalen av Urema Graben och markerar den nordvästliga gränsen till Gorongosa Nationalpark. Parken har ett brett ekosystem av flodplan, grässlätter och träd.

Studien fokuserar på den västra marginalen och är baserad på resistivitetsmätningar, ytliga borrhål för jordprov samt bestämning av avrinning för att erhålla mer information om de hydrologiska förhållandena i området.

Resultatet från resistivitetsmätningarna visar att området är förkastat och har ett infiltrationsområde. Från marginalen ut mot dalgången indikerar resistivitetsprofilerna att den solida gneissen blir uppsprucken och eroderad, därefter finner man sandsten. De översta ~10-15 m inom hela området består av ett högresistivt lager och tolkas som alluvial sand. Detta lager sträcker sig från marginalen över gneissen och in i dalgången. Med resultatet från resistivitetsmätningarna ser man att sandstenen lutar från marginalen mot sydost. Längre ner in i dalgången är de alluviala sedimenten underlagrade av lågresistiva linser bestående av silt/lera, som i sin tur är underlagrade av ett medium-resistivt lager av sand.

Den översta alluviala sanden utgör en öppen akvifär, under denna utgör gneissen en hydraulisk gräns, medan den spruckna gneissen är en öppen sprickakvifär. Linserna utgör en akviklud som underlagras av sand och representerar en semi-öppen akvifär. Det understa lagret som utgörs av sandstenen är en por-sprickakvifär.

Avrinningsmätningarna visar på en stor förlust av vatten nedströms vilket indikerar att ytvattnet infiltreras ner till akvifärerna och transporteras i en sydostlig riktning.

Nyckelord: Moçambique, Geofysisk undersökning, Gorongosa Nationalpark, Grundvattenbildningszon, Nhandugefloden, Urema Graben.

Li Stenberg, Institutionen för geo– och ekosystemvetenskaper, enheten för geologi, Centrum för GeoBiosfärsvetenskap, Lunds Universitet, Sölvegatan 12, 223 62 Lund, Sverige. E-post: li.stenberg@hotmail.com

1 Introduction

Gorongosa National Park (GNP) is located within the Urema drainage basin of central Mozambique, which is situated in the southernmost extenssion of the East Africa Rift System (EARS). The water resources in the National Park are indispensable for the function of the ecosystem and the balance between floodplains /grasslands and woody coverage. This is essential for the high biodiversity and animal population of the area. The water resources merge in Lake Urema, which is located in the valley floor of the Urema Graben in the central part of Gorongosa National Park. Lake Urema, the heart of the National Park, is a shallow natural lake that expands to more than 200 km^2 in high flood seasons and recedes to between 12 and 15 km^2 during the dry seasons. Water from seasonal channels feeds Lake Urema during the high flood season, while the Vunduzi river and the Nhandugue river supply Lake Urema with water all year (Fig. 2).

A long-term project has been initiated by the Gorongosa National Park, where one of the main goal is to gather additional knowledge and information about the geology and hydrology in the area of the Nhandugue River. The changes in the region can be traced to human impact, as extensive farming, dam construction and industry. A direct consequence of these impacts are an increased risk of desiccation of Lake Urema. The ambition is to be able to predict changes in the environment that may affect the future of Lake Urema. This project has been described in the *Long-term plan for hydrological research: adaptive management of water resources at Gorongosa National park* (Beilfuss et al. 2007).

A previous study was conducted in the downstream area of the Urema floodplain in 2008 to investigate if it was possible to perform resistivity measurements in the area, the results were presented in the master thesis *Geophysical investigations in a part of Gorongosa National Park in Mozambique* (Chirindja and Hellman 2009).

Investigations, such as resistivity and conductivity measurements and ground surveys used in this investigation, will give complementary and important information about the assumed main ground water recharge areas at the lateral margins of the Urema Graben and the Quaternary sediments. This fieldwork was preformed together with Kristina Arvidsson in three areas and will result in two master theses (45 ECTS credits). This thesis will process the information concerning upstream Area 1 and middle Area 2 while Kristina Arvidsson also will deal with the middle area and downstream Area 3. The results from our fieldwork will thus be presented in two separate thesis; *Geophysical and hydrogeological survey in a part of the Nhandugue River valley, Gorongosa National Park, Mozambique – Area 1 and 2* by Li Stenberg and *Geophysical and hydrogeological survey in a part of the Nhandugue River valley, Gorongosa National Park, Mozambique – Area 2 and 3* by Kristina Arvidsson.

The aim of this thesis is to present new data for upstream Area 1 and middle Area 2 to increase the knowledge about the geology and hydrogeology. The following questions will be addressed;

- Is there any evidence of tectonic activity in the area?
- Are there any differences in mineralogy and/or carbonate content in Area 1 and 2? Provenance?
- How thick are the Quaternary sediments and by what process were they deposited? Can any differences in thickness be observed between the two areas?
- What types of ground water reservoirs are located in the two areas?
- What type of sediment is located beneath the Quaternary sediment? May this have a impact on the water flow?
- Is the surface water in the area being infiltrated and is the ground water being infiltrated down to deeper aquifers?

Fig. 1 Map over southern and central parts of Mozambique in Africa. Gorongosa National Park is located in the central part and marked with green colour. (after Danish Institute For Human Rights, 2006 and GNP 2009).

2 Background

2.1 Study area

Mozambique is located in southern Africa (Fig. 1), enclosed by the Indian Ocean in the east and southeast, Tanzania, Malawi and Zambia in the north and Zimbabwe, South Africa and Swaziland in the west.

Gorongosa national park is situated within the Sofala province at 19°S and 34°W in the central part of Mozambique. The park covers approximately 5370 km^2 (GNP 2009) and have four different landscape variations: the Urema Graben, the Gorongosa Mountain, the Báruè Platform and the Cheringoma Platform (Fig. 2).

The area contains two major features that are of importance to the Gorongosa ecosystem, the water received from the Gorongosa Mountain and the obstructing alluvium sediments of the Muaredze River at the outflow of Lake Urema. The Muaredze River and the Urema drainage meet on the Cheringoma Platform (Fig. 2) and form the main critical elevation that control the drainage of the Urema Graben, which in turn controls the outline of the rift Valley floor (Tinley 1977).

The study of the two areas was concentrated to the Nhandugue River area (Fig. 3) during the dry season, located at the northern boundary of the park (Fig. 2). This is where the river meanders from the Báruè Platform north of Mount Gorongosa, into the Urema Graben and the GNP.

2.2 History and Restoration project

In 1498 the first Portuguese arrived in what is today considered Mozambique, and during the 16th century they controlled all trade. A century later the first Portuguese settled and began colonizing the region (Halkjaer 2007). Hunters, explorers and naturalists were attracted to the Gorongosa region because of the magnificent wildlife, and 1920 a bit of land was ordered to become a game preserve. In 1935 Jose Ferreira became the parks first guard protecting the wildlife (GNP 2009), while a headquarter was established in Chitengo 1951. The number of tourist increased continuously and in 1960 the Gorongosa Park was named a national park by the government of Portugal. Four years later the Mozambique Liberation Front started a war of independence against the Portuguese that lasted until 1975, upon when Mozambique become an independent country (Halkjaer 2007). The war had little effect on the daily life in Gorongosa National Park, and at this point the park had the largest population of lions in all of Africa (GNP 2009). However, the peace did not last and in 1983 a civil war

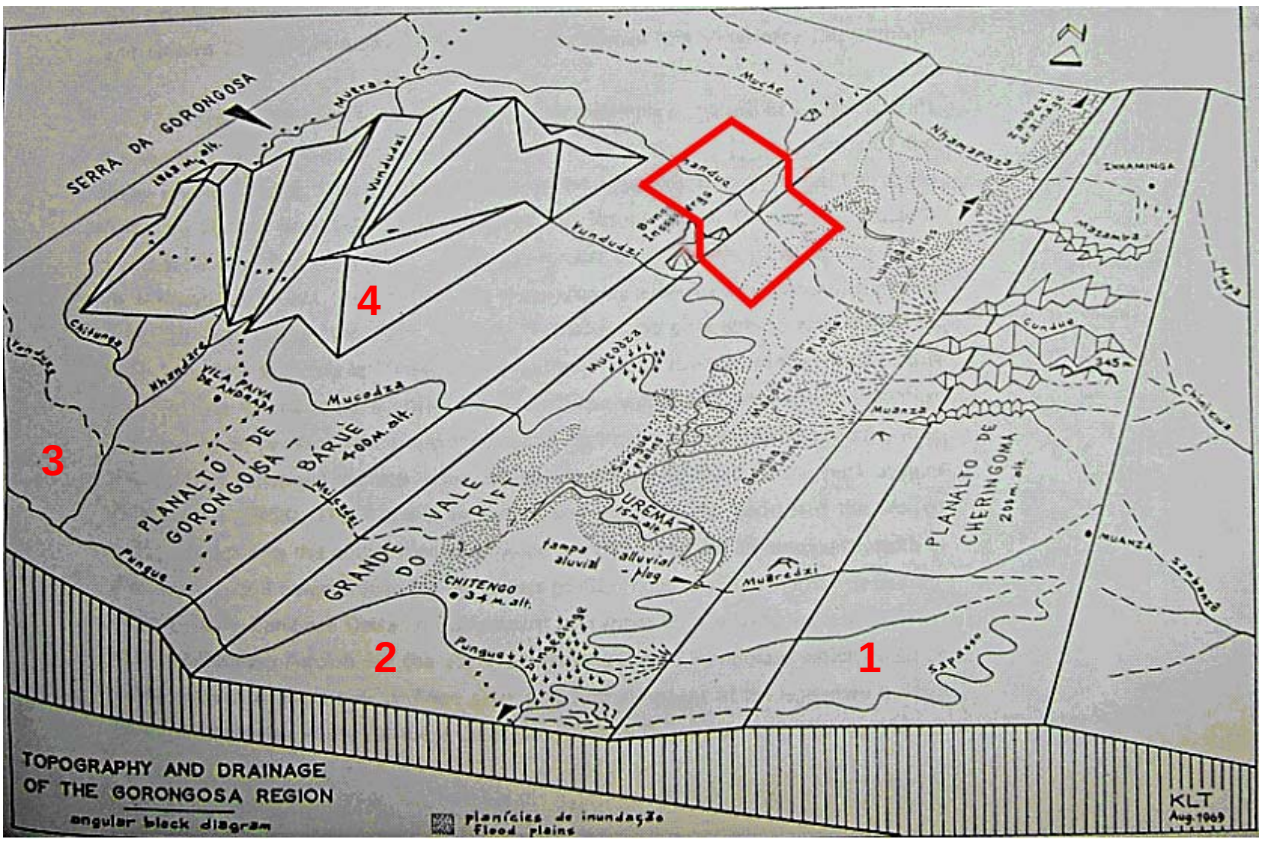

Fig. 2 Block diagram display the four different landscapes of the Gorongosa region and drainage pathways to the rift valley floor (Urema Graben). The figure illustrate Cheringoma Platform (1), Urema Graben (2), Báruè Platform (3) and the Gorongosa Mountain (4) from east to west. The red square marks the study area within the western rift margin at the Nhandugue River (Tinely 1977).

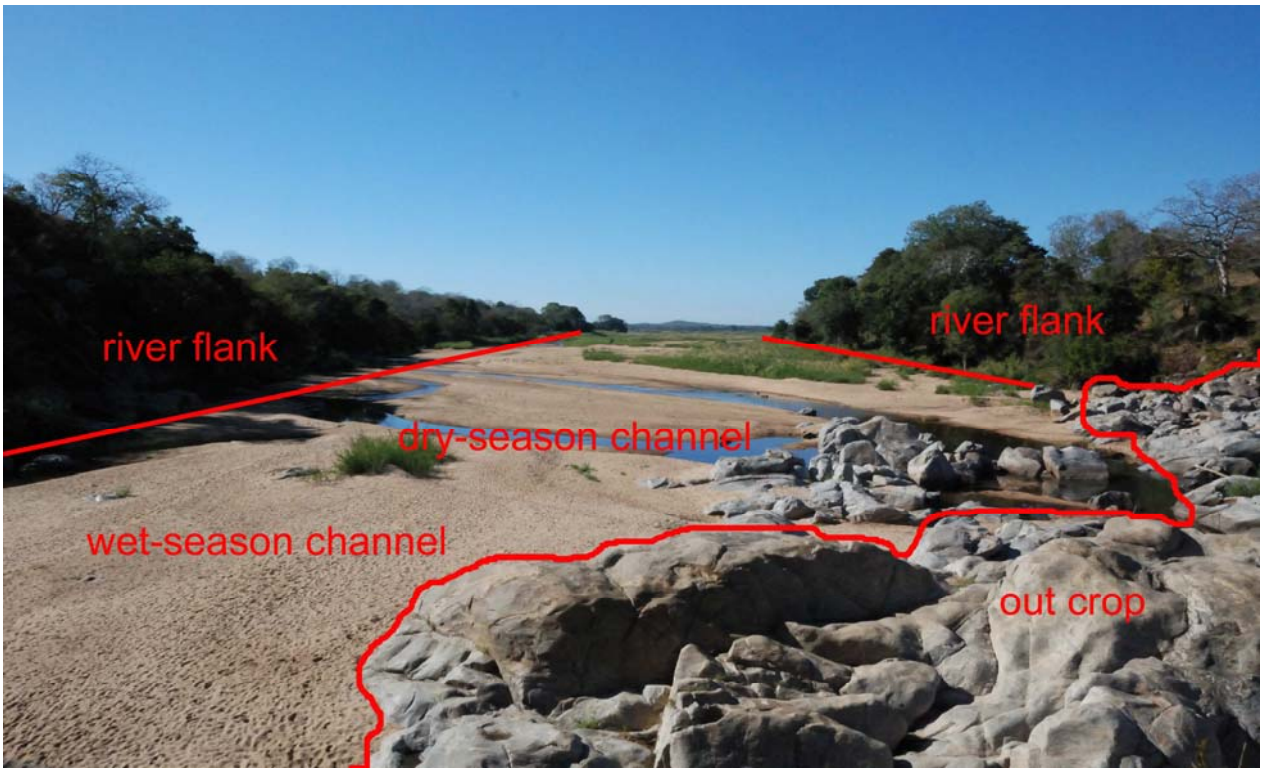

Fig. 3 Photo of Area 1 displaying the division of the Nhandugue River area during the dry season: (i) an outcrop (ii) a dry-season channel (iii) a wet-season channel and, (iiii) river flanks on each side of the wet-season channel. The width of the channel is approximately 200 m.

broke out, resulting in Gorongosa National Park becoming a battlefield and consequently being deserted during the following nine years of war. By 1992, as the civil war ended, the large mammal population of the park had been reduced by 90 percent (GNP 2009). The rebuilding of the Gorongosa National Park started in 1994 by the African Development Bank, and during the following five years this project resulted in new roads and the training of new guards to stop the illegal hunting that threatened the park. The Carr Foundation agreed to assist the park in 2004 and is still today founding the continuous restoration of the park (GNP 2009).

In 2007 a long-term plan for hydrological research was developed initiated by the Gorongosa National Park, with the goal of biodiversity conservation, sustainable development and adaptive management of natural resources in the region (Beilfuss et al. 2007)

2.3 Geology

2.3.1 Regional geological development

The complex geology of Mozambique was initiated during its crustal development in the Eoarchean (4000 – 3600 Ma) and the Paleoarchean (3600 – 3200 Ma) that later would outline the foundation of the supercontinent Gondwana. In the Mesoarchean (3200 - 2800 Ma) and the Neoarchean (2800 – 2500 Ma) the formation of the granite-greenstone, cratonisation and the mobile belt took place. During the Proterozic (2500 – 542 Ma) the area suffered several tectonic cycles, the last being the Pan-African early Paleozoic cycle, characterized by granitic-monzonitic-syenitic intrusive magmatism. During this cycle the centre of Gondwana was located in the position of modern South Africa. The end of the Neoproterozic and Early Paleozoic is represented by denudation, which was occasionally interrupted by tectonic and magmatic events (Lächelt 2004).

The Karoo, which corresponds to the Gondwana period (300 – 175 Ma), can be divided into two periods: the Gondwana Rifting Phase (300 – 205 Ma) and the Final Phase (205 – 175 Ma). The development of the rift structures and platform depressions occurred during the Gondwana Rifting Phase, while the Final Phase is represented by the sea-floor spreading and finally the breakup of Gondwana Supercontinent. This was followed by the Post Gondwana Period, which consist of three subphases: break up of Gondwana (175 – 118 Ma), stabilisation (118 – 35 Ma) and neorifting (35 Ma to Recent) (Lächelt 2004).

In the first subphase, the active sea-floor spreading divided the supercontinent into a eastern (Australia, Antarctica, India, Sri Lanka, Madagascar, the Seychelles) and a western (Africa and South

America) region approximately 130 Ma. As Africa finally broke off from South America, a second transgression occurred (118 Ma). During the stabilisation phase, India and the Seychelles split off from Madagascar and carbonate sediment were deposited in the surrounding shallow-water. In the neorifting phase, the EARS was formed. Regressions then dominated in the area during the Oligocen, but were interrupted by a transgression in the Miocene. This transgression, which resulted from active tectonic movements and the formation of grabens, formed thick sediment beds of siliciclastic material. During the Miocene, the shallow-water shelf was uplifted and continued to be exposed during the Holocene (Lächelt 2004).

2.3.2 Local Geology

2.3.2.1 Urema Graben

The Urema Graben, which comprises the southernmost extension of the EARS, is a rift approximately 40 km wide dividing the Báruè Platform in the west from the coastal plain of Cheringoma Platform in the east (Fig. 4). The Graben consists of faults trending N-NE to S-SW and have high and steep sides in the north, while the southern part is shallow with relatively low angled slopes. The rift valley floor is the lowest part of the Urema Graben and consists of alluvial sand, silt and gravel (DNG 2006).

The area where the Pungwe River flows out into Lake Urema represents the lowest elevation of the basin (12 m. a. s. l.) (Tinely 1977).

The fault structures are characterized by half-grabens (Fig. 5), which constitute an important influence on the sedimentdistribution (Crossley 1984). The half-grabens are connected by single normal faults, and the basement of the hanging wall is detached from the footwall. The footwall is the main source of sediments to the adjacent hanging wall, while the eroded material of the hanging wall will have a larger spread. At the fulcrum the displacement is zero (Leeder & Gawthorpe 1987).

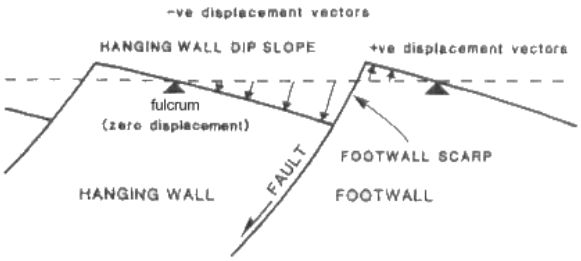

Fig. 5 Diagram for a tilt block/half-graben. The main tectonic slopes that are formed during basin development. The position where displacement is zero is referred to as the fulcrum, the transition from areas of the hanging wall undergoing positive motion due to footwall uplift to areas undergoing negative motion due to hanging wall subsidence (Leeder & Gawthorpe 1987).

2.3.2.2 Báruè Platform

The Báruè Platform is located to the west of the Urema Graben. A fault divided the Báruè Platform from the Urema Graben and was probably created during the Jurassic, but has been refractured later on. The fall line drops to the basin floor in a low grade angle, but the crystalline bedrock occurs as hills across the basin floor at the boundary between the Báruè Platform and Urema Graben. The Báruè formation has been eroded by the fluvial activity (Tinely 1977).

Báruè Platform is divided in tree groups: Báruè Supergroup, Lupata group and Sena Formation. The Báruè Supergroup is characterized by five types of Pre-Cambrian metamorphic granitic and migmatitic gneisses, and form the Báruè Platform and the western edge of the Urema Graben. These are the oldest rocks in the region (>570 Ma) (Tinely 1977).

The Lupata group consists of conglomerate

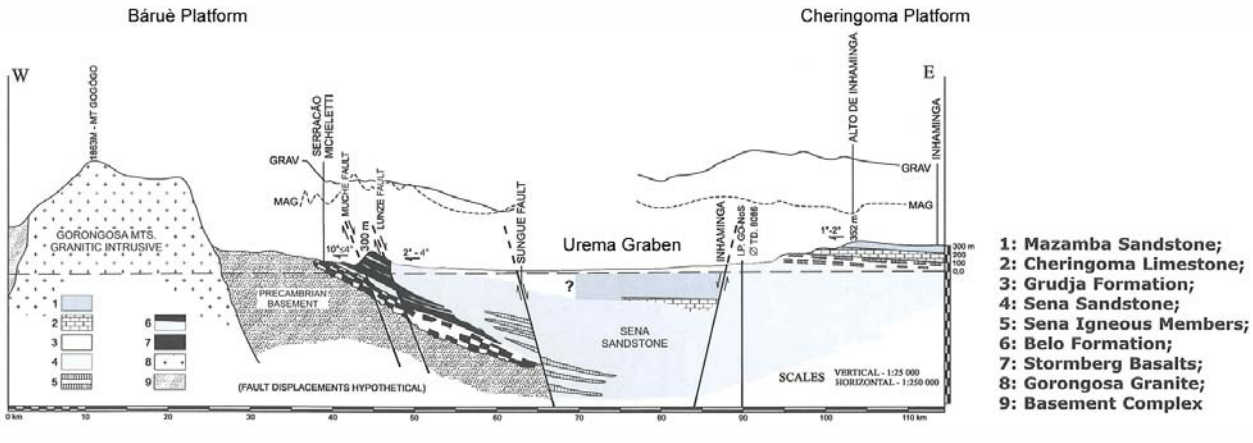

Fig. 4 Vertical cross-section of Urema Graben. Stretching from the Gorongosa Mountain at the Báruè Platform in the west to Cheringoma Platform in the east (after Lächelt 2004).

sandstone and Phonolitic lava. The conglomerate in the sandstone consists of fragments from the surrounding intrusive bedrocks, cemented by argillaceous-calcareous and tuffaceous material. The weathered sandstone consist of a red sandy clay, with calcium rich subsoil (Tinely 1977).

The Sena Formation is characterized by very thick sediments of sandstone (~3000 m) mainly of continental origin that formed during the Lower to Middle Cretaceous. The lower section of Sena Formation also contains shells of fish, calcareous schists from arthropodes and plant remains. The sediments of the Sena Formation constitute coarse to medium arkose sandstone, while the matrix is calcic-argillaceous. The colour is often beige, yellow-grey or reddish. As the Sena Formation is eroded, the end result is sand and calcareous sandy clay. The layer-silicate clay, montmorillonite, is a result of erosion of the associated mica (Tinely 1977).

2.3.2.3 Cheringoma Platform

The Cheringoma Platform is located to the east of the Urema Graben and it is tilted approximately 3-5^{o} to the SE. It has been eroded from primarily two sides, by riftward and seaward drainage. The platform is younger than the Báruè Platform. The Cheringoma Platform has a sharp fault line and consists of Cretaceous and Tertiary sediments: Mazamba Formation, Cherigoma Formation, Grudja formation, and Sena Formation (Tinely 1977).

The Mazamba Formation consists of arkosic sandstone, which is partly conglomeratic, and the Inhaminga sandstone that consists of a coarse to medium coarse arkose sandstone with conglomerate horizons. This sandstone is mostly cemented by calcic-argillaceous matrix, but occasionally by silica. The Cheringoma formation (54 Ma) represents warm water facies, characterized by Eocene fossiliferous sediment of white to pink calcareous limestone. It is about 70 m in thickness and contains an abundance of the foraminifera genus *Nummulites*. The Grudja formation is about 200 m thick yellowish-green glauconite sandstone that is primarily defined by *Lopha ungulta* shell fossils. The Sena Formation is about 70 m thick and the of same type of sandstone that is found in the Báruè Platform (Tinely 1977).

A primary feature of the Cheringoma Platform is termite hills that have a major impact on geomorphology, hydrology and ecology in the region (Tinely 1977).

2.3.2.4 Gorongosa Mountain

Gorongosa Mountain was formed during the late Jurassic to early Cretaceous, and is located within the Báruè Platform, containing both alkaline and acidic plutonic intrusion. The Báruè Platform was initially penetrated by an intrusion of gabbros, and at the contact surface between the bedrock and the intrusion, pyroxene and amphibolite hornfels formed. Dolorite dykes of the same composition and age as the intrusions have also been found. They have a N-S direction that penetrate the gneisses in the old foliations or weaknesses of the bedrock (Tinely 1977).

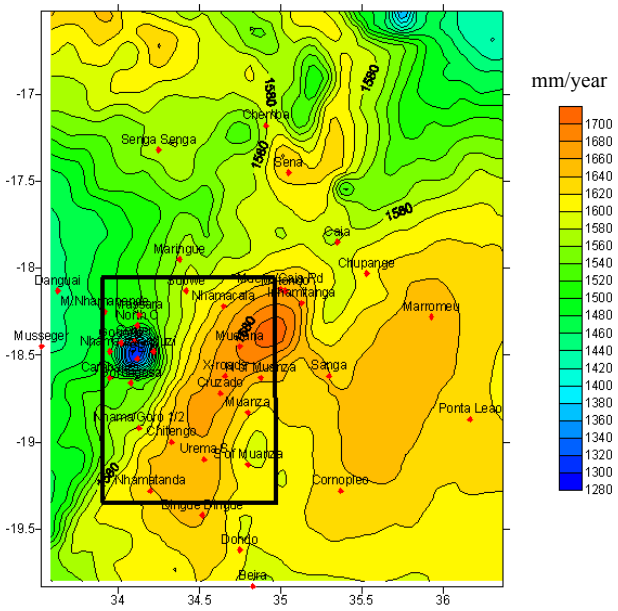

Fig. 6 Map showing annual potential evapotranspiration. Gorongosa Moutain has the lowest evapotranspiration (1280 to 1320 mm/year) while the Urema Graben has the highest evapotranspiration (1620 to 1680 mm/year). The black rectangle marks the area of interest (Owen 2004).

The sandstone, basalt and rhyolite in the NW area represent the Karoo period (between 300 and 175 Ma), and the morphology of these sediments is slightly undulating and slopes to east towards the Cretaceous sediments. When the sandstone is eroded it becomes sand, while the feldspars turn in to sandy clay or clay, and the basalt becomes silicate and gritty clay (Tinely 1977).

The Gorongosa Mountains highest point is the Gogogo peak, (1863 m.a.s.l.) and is a Cretaceous granitic intrusive complex with gabbro and granite extending 30 km in N-S and 20 km in E-W direction (Böhme 2005). The structure on the mountain is tectonically controlled (Steinbruch & Vogler paper in preparation).

2.4 Climate and Hydrology

2.4.1 Climate

Central Mozambique is included in Köppen's Tropical Savanna Climate, but the Gorongosa Mountain belongs to Warm Temperate Rainy Climate (Tinely 1977).

The factors controlling the climate in Central Mozambique during the summer are anticyclone (high pressure) systems and the low pressure areas (South Indian Ocean high). The high pressure cell is located over the Asian landmass, and the low pressure is located between Africa and Australia. The Asian air masses emerge from south and follow an ocean path; this moist air mass is called the northeast monsoon. In

addition, another branch of the high pressure cell is taking the path over the central-east Africa (Beilfuss et al. 2007).

The Urema Graben in central Mozambique is an area of low atmospheric pressure, due to high temperatures caused by heating of the Earth's surface. This results in very dry winds and a temperature that is on average 25-30°C during the summer (Beilfuss et al. 2007). During the winter the Intertropical Convergence Zone (ITCZ) moves and the South Indian Ocean moves in a northwestern direction, resulting in southeast trade winds (Tinely 1977). The temperature during the winter is usually between 20-25°C (Beilfuss et al. 2007).

2.4.2 Water balance — evaporation and precipitation

The Urema Basin has an annual rainfall of 600-1000 mm/year (Owen 2004), with the main precipitation falling between October and April while the dry season take place between May and September. The maximum average annual evaporation is measured in the area of the Urema Graben, while minimum values are recorded at the Gorongosa Mountain (Fig. 6). During the dry season, evaporation can exceed more than 1000 mm/year, which lead to water deficit. However, the Gorongosa Mountain experience high precipitation, at a total of 1800 to 2200 mm/year, and due to steep slopes and bare rock the inflow of water is continuous during the year (Beilfuss et al. 2007).

According to Owen (2004) the recorded rainfall data (Fig. 7) indicate that the Gorongosa Mountain area have the highest annually rainfall (2000 mm/year), followed by the Cheringoma Platform (1000 to 1400 mm/year) and then the Báruè Platform (800 to 1200 mm/year). The Urema Graben experiences the least amount of precipitation compared to the rest of the area, while being related to swampy areas and shallow lakes, like Lake Urema, due to the gentle slopes.

2.4.3 Hydrogeology and ground water

Water is transported to the valley from the Gorongosa Mountain, while the Báruè Platform has fracture-controlled aquifers and Cheringoma Platform contains karst and pore aquifers (Owen 2004).

The sandstones generally have a higher permeability than the crystalline bedrock in the Báruè Platform. The ground water of the Báruè Platform has been infiltrated in the coarser sand fraction that exist in the rift margin. The two larger streams, Vunduzi and Nandugue, provide the Urema Graben with surface water that flow through the rift into the Pungwe drainage (Owen 2004).

Gorongosa Mountain has its own microclimate as a result of its high elevation and the total precipitation. The rift flanks experience less rainfall than the Gorongosa Mountain, but higher quantities than the Urema Graben, where the water is drained. The northern part of the Cherigoma Platform is characterized by numerous pans and sinkholes that interrupt the normal drainage, as the water flows through the high perme-

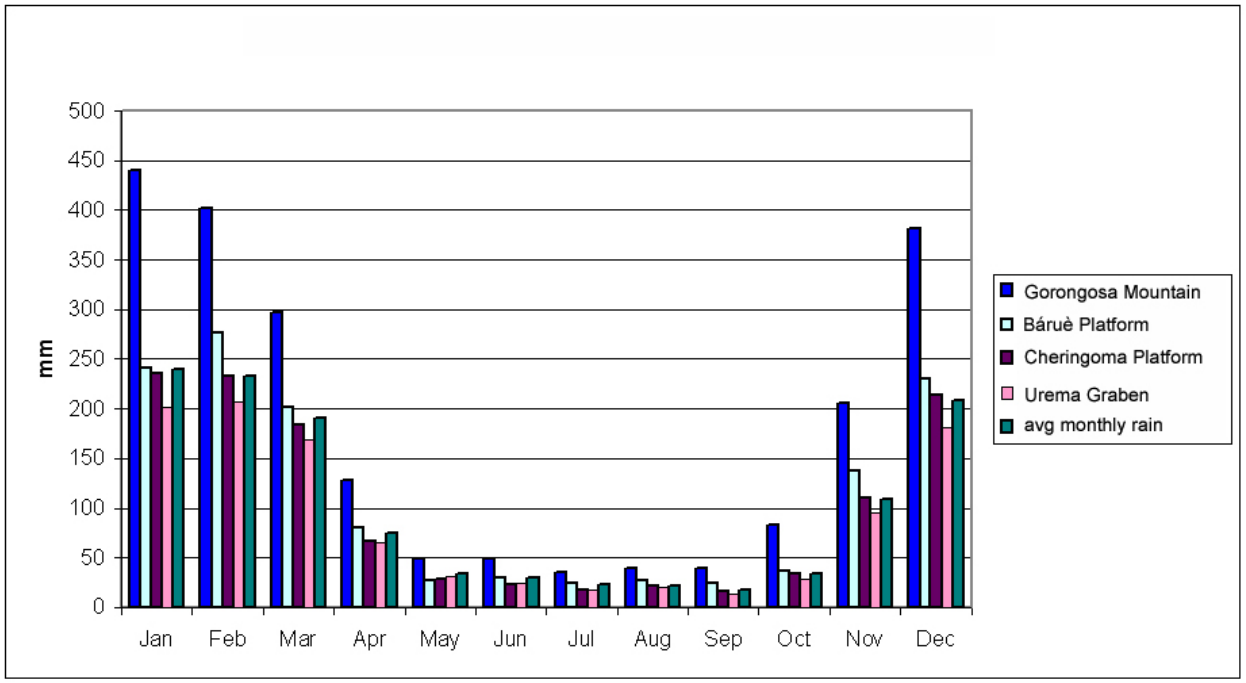

Fig. 7 Diagram displaying monthly rainfall in the different landscapes. Gorongosa Mountain area have the highest annually rainfall (2000 mm/year) followed by the Cheringoma Platform (1000 to 1400 mm/year) and then the Báruè Platform (800 to 1200 mm/year). The Urema Graben has the lowest rainfall of the area (after Owen 2004).

able sediments and infiltrate the ground water. The Báruè Platform has a dendritic drainage pattern, however, the orientation of the lineament controls the water flow to some extent. The crystalline bedrock also has a much lower permeability (Owen 2004).

The main factor controlling the hydrology and the relationship between rainfall, runoff and infiltration is the geology in the area. Critical factors include the degree of fracturing of the bedrock, as well as the thickness of weathered layers (Owen 2004).

2.4.4 The Urema drainage basin and Nhandugue River

There are three main rivers originating from the Gorongosa Mountain: Nhandare, Muera and Vundudzi rivers. The Nhandare river runs in a S-N direction from the foot of the mountain out on to the Bàrué Platform, ultimately flowing out into the Punga River in the north. The Muera River is a tributary of the Nandugue River, while the Vundudzi River flows out into Lake Urema after crossing the Urema Graben. On the valley floor all major drainage originate from inland, and have a SE direction. The fractures and the dip of the underlying bedrock is the main controlling factor of the valley floor drainage (Tinely 1977).

The Gorongosa Mountain supplies the drainage on the rift valley floor with water, but the escarpment of the Urema Graben and land use is likely to affect the hydrology in the area. For example land clearing and deforestation are likely to increase the runoff and decrease the evaporation (Beilfuss et al. 2007).

Nhandugue River is located north of the Gorongosa Mountain. The flow of the Nhandugue River is seasonal and depends on precipitation (Tinely 1977), and as it reaches the margin of the rift valley floor it forms 20 km wide alluvial fan. This large fan is created by high amount of sediment, resulting mechanical weathering in combination with a high sedimentation rates. The main minerals being deposited here are quartz, mica and feldspars that originate from the gneisses and migmatites of the Báruè Platform (Böhme 2005).

As the Nhandugue River reaches the rift valley floor, the angle of the slope is drastically reduced from ~0.3° to ~0.07°. This results in the formation of several confluents that cover ~68% of the entire catchment area of the Lake Urema (Böhme 2005).

3 METHODS AND MATERIAL

During the course of this study the following methods have been used; geophysical surveying, including resistivity and induced polarization (IP); ground surveying, including sieving, hydrometer analysis, calcium carbonate content, mineral content and loss on ignition. In addition, discharge surveys were also preformed. The different methods will be discussed in this section.

3.1 Resistivity

The resistivity profile was located along the river channel to get a better picture of the Quaternary sediments within the channel, and determine the possible presence of aquifers.

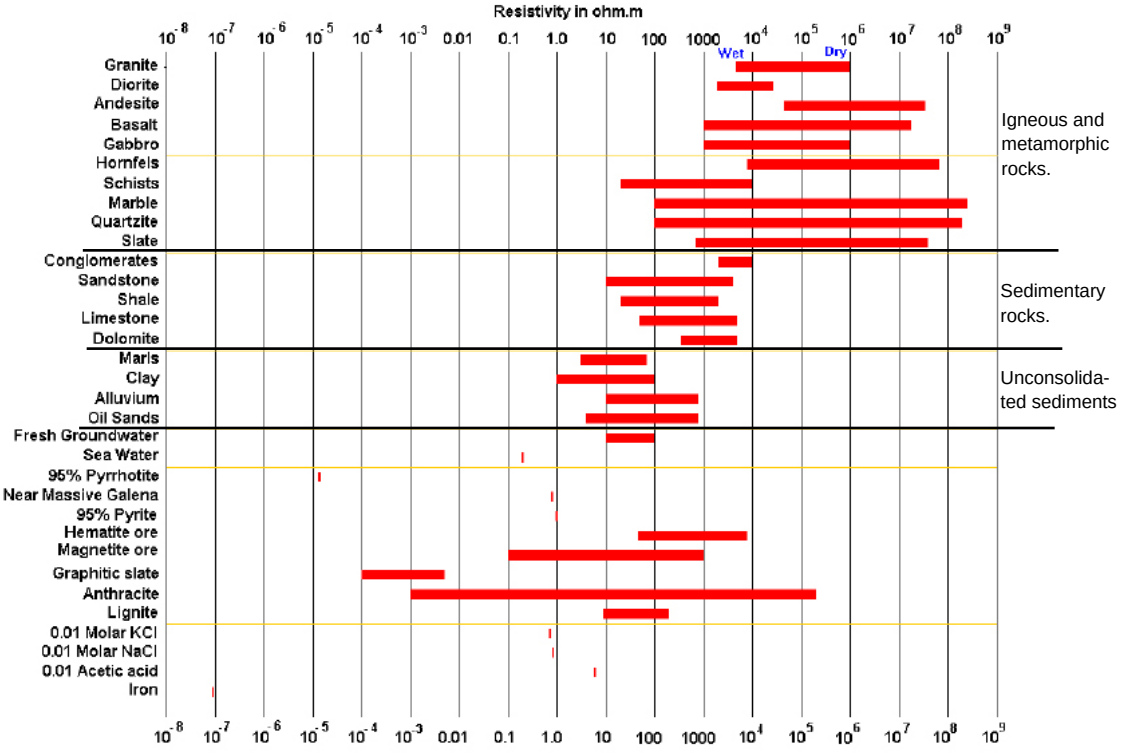

Fig. 8 Diagram displaying characteristic resistivity intervals for different material (after Loke 2004).

3.1.1 History and geological material

The origin of the resistivity method dates back to the 1920's with the first experiments performed by Conrad Schlumberger in the fields of Normandy (Sharma 1986). Resistivity is a popular method within electrical exploration because of its capability to produce images of the subsurface, and because of its user friendly inversion software (Dahlin & Zhou 2006). Resistivity measurements have been used for many decades in hydrological, mining and geotechnical investigations (Loke 2004). The resistivity method involves measuring the grounds ability/inability to conduct current by sending electricity through the ground. Porosity, degree of water saturated pores, resistivity of pore fluids, mineral composition and mineral structure are parameters that affect the resistivity in a geological material (Jeppsson 2004). As a result, resistivity is a parameter that is influenced by different variables (Sharma 1986) and may vary not only between geological formations but also within a formation. A broad review of resistivity properties of different geological material is illustrated in Fig. 8.

The interval of the resistivity can reflect more than one geological material, which makes the identification of different materials difficult (Jeppsson 2004). For example, sandstone has a value of 10 to 10^4 Ωm, while clay has a value of 1 to 1000 Ωm. To get the correct geological information from resistivity measurements it is important to have good knowledge about the local geology, as well as being able to interpret typical resistivity data. Sedimentary rocks usually have higher water content as a result of higher porosity, which is reflected by normally lower resistivity values (Loke 2004).

3.1.2 Background

There are two types of resistivity: true and apparent resistivity. The apparent resistivity is the resistivity obtained by measuring an inhomogeneous subsurface (Reynolds 2006), but in a homogeneous ground it is equal to the true resistivity (ABEM 2009). The true resistivity can be estimated by a model process. Ohm´s Law is fundamental in resistivity surveys; it is controlling the flow of current in the ground (Loke 2004). A controlled current (I) is transmitted between two electrode into the ground, while the potential (U) is measured between two other electrodes. The resistivity (R) is given by the Ohm's Law (equation 1.1) (ABEM 2009):

$$R = \frac{U}{I} \qquad (1.1)$$

The SI unit of the Ohm´s Law is ohm meter (Ω m) (Sharma 1986). The resistivity of a material ρ, is equal to the inverse conductivity σ ($\rho = 1/\sigma$) (Loke 2004) and related to the resistance by a geometrical factor (K) (ABEM 2009). The apparent resistivity ρ_a of a subsurface can be calculated using:

$$\rho_a = K \cdot \frac{U}{I} \qquad (1.2)$$

a combination of equation (1.1) and (1.2) will give equation 1.3:

$$\rho_a = K \cdot R \qquad (1.3)$$

The geometrical factor (K) can be calculated by the knowledge of the configuration and distance between the two current electrodes (*C1 and C2*) and the potential electrodes (*P1 and P2*) (Fig. 9). The geometrical factor (K) is (Loke 2009):

$$K = 2\pi \cdot \left(\frac{1}{r_{C1P1}} - \frac{1}{r_{C2P1}} - \frac{1}{r_{C1P2}} + \frac{1}{r_{C2P2}} \right)^{-1} \qquad (1.4)$$

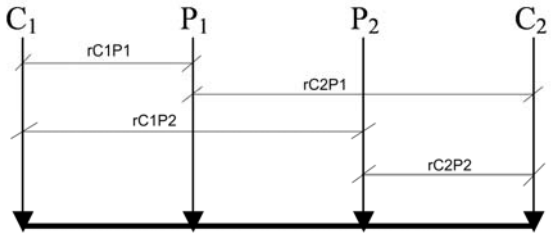

Fig. 9 Schematic electrode arrangement, with two current electrodes (C1 and C2) and two potential electrodes (P1 and P2), also showing the distances need for calculation of the geometrical factor (K) (Chirindja & Hellman 2009).

3.2 Induced Polarization

Induced Polarization (IP) was introduced by Conrad Schlumberger in 1912 and been used since the 1940s.

IP depends on the distribution of mineral grains in soil and bedrocks (Reynolds 2006) and measure the grounds ability to polarize (Jeppsson 2004), called the IP-effect. The IP-effect can be compared with a

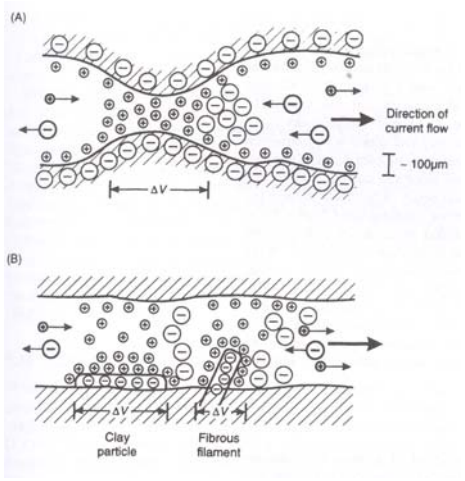

Fig. 10 Development of membrane polarization associated with (A) a constriction within a channel between mineral grains, and (B) negatively charged clay particles and fibrous elements along the sides of a channel (Reynolds 2006).

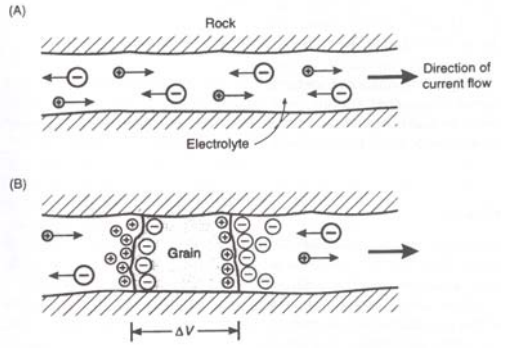

Fig. 11 Grain (electrode) polarization. (A) Unrestricted electrodes flow in a open channel. (B) Polarization of an electronically conductive grain, blocking a channel (Reynolds 2006).

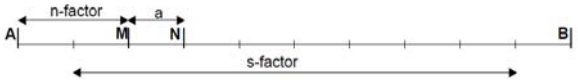

Fig. 12 Sketch of gradient configuration with a separation (s+2)a, displaying the position of the electrodes for a measurement with s-factor 8 and n-factor 2 (ABEM 2009).

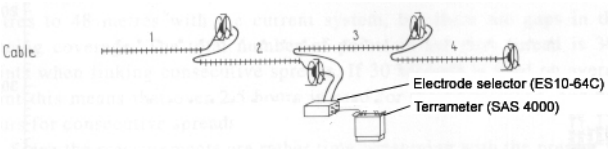

Fig. 13 The set-up of instrument with the electrode selector and terrameter in the centre. (after Dahlin 1993).

capacitor, which is charged when current is switched on and discharges when current is turned off (Dahlin 1993). Membrane polarization (Fig. 10) and electrode polarization (Fig. 11) are the two main mechanisms that cause a polarization process.

There are two reasons for membrane polarization: the size of the pore channel and the presence of clay in the channel (Reynolds 2006). Minerals with a small diameter, e.g. clay, have negative charge, and hence attract positive ions. As a result, a positively charged layer, approximate 10^{-5} mm thick, decreases the pore diameter and can block the smallest pores. When this has sustained a stable local polarization, the voltage is switched off and causes a decay of local polarization that in the end reaches zero, thus causing a measurable IP (Jeppsson 2004).

The electrode polarization effect is caused by the ionic balance being disturbed, which in turn causes a current flow due to applied voltage (Reynolds 2006).

There are two types of IP measurement: Time-domain and frequency-domain measurements. In this study the data collection was performed with time-domain measurement. During this type of measurements, a direct current (DC) is lead through the ground and the data from the variation in voltage is studied. This variation can be present in mV/V or %, which is defined as chargeability (Reynolds 2006). There is a strong correlation between the chargeability and the resistivity. To improve the interpretation of IP anomalies normalized chargeability is used. The normalized chargeability is defined as the chargeability divided by the resistivity magnitude and present in mS/m (Slater & Lesmes 2002).

To combine resistivity and IP measurements is not a problem, because IP and resistivity can be measured using the same configuration (Reynolds 2006), and measurement of resistivity is included in IP measurement (Jeppsson 2004).

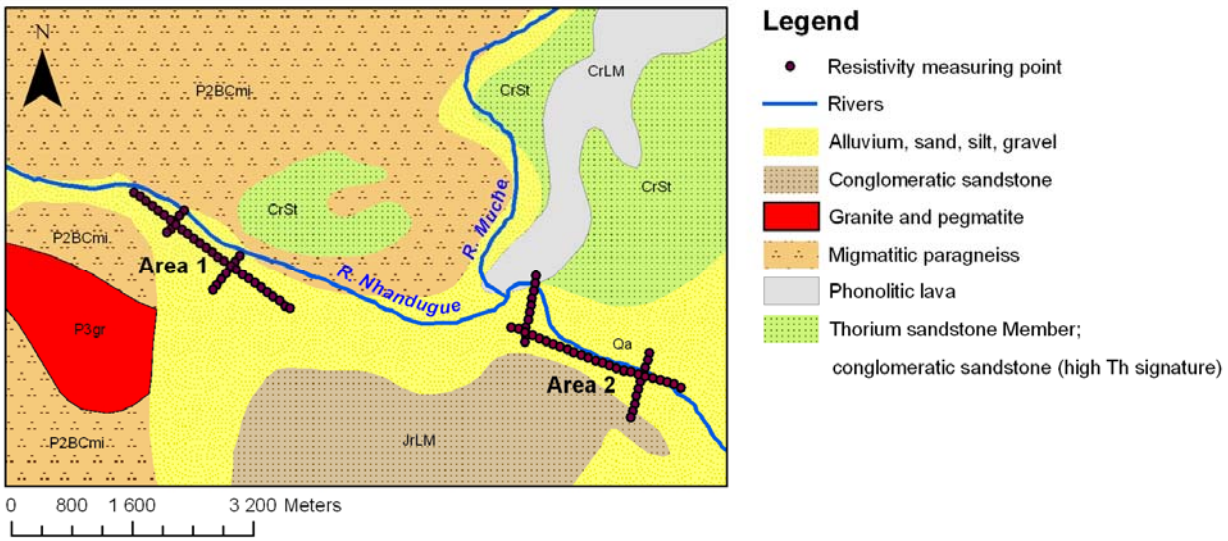

Fig. 14 Overview of Area 1 and Area 2. The name in the bedrock correspond to the Geological map (Appendix 1). Due to natural variations in the position of the Nhandugue River with season and between the years, the map shows a mean position of the river. Therefore a slight inaccuracy occurs in the location of the resistivity profiles in relation to the river as it was during the fieldwork.

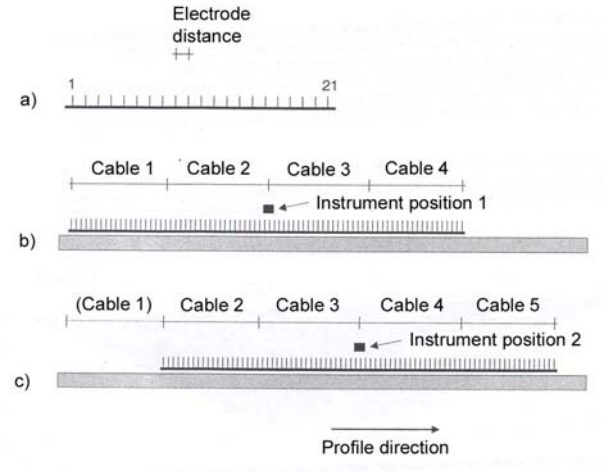

Fig. 15 Multiple gradient configuration, a) Cable with equal distance between the 21 electrodes. b) four cables are connected with the instrument at instrument position 1 in the middle, c) the instrument is moved from instrument position 1 to instrument position 2 and cable 1 is moved to cable position 5 (Jeppsson 2004).

3.3 Data collection

The data collection of resistivity and IP in the six profiles (Fig. 14) was performed, with multiple gradient configuration continuous vertical electrical soundings (CVES) roll-along measurements. The CVES is based on the Lund Imaging System, a system developed for high-resolution 2D and 3D survey (ABEM 2009) that is measured on a large number of electrodes connected by cables (Jeppsson 2004). The multiple electrode gradient survey is performed by sending a current with a (s+2)a separation (Fig. 12), at the same time reading the potential differences between the potential electrodes with spacing "a" (Dahlin & Zhou 2006). In multiple electrode gradient surveying there is a large number of current electrode used with different spacings of "a" and/or "s" (Dahlin & Zhou 2006). A larger spacing of the current electrodes gives a deeper penetration, while a smaller spacing of the potential electrodes gives the potential variation in more detail (ABEM 2009).

The gradient configuration is partially similar in characteristics to a pole-dipole configuration (ABEM 2009). In a pole-dipole configuration, one of the current electrodes is located at a large distance, i.e. a minimum of 10 "a" (Jeppsson 2004). When the potential dipole is placed in the centre of the current electrodes the configuration is identical to the Schlumberger configuration (ABEM 2009).

The measurements were performed on different configurations resulting in different penetration depth on different points (Jeppsson 2004). A complete series contain more than 1000 measure points.

The fieldwork was conducted in the following steps: Four 100 m cables, holding 21 electrodes take-out at 5 m spacing were rolled out in a serial formation, with the instrument in a central position (Fig 13). An electrode was placed in the ground at each take-out on the cable and connected to the cable with jumpers (small cable). The last and the first take-out were laid out to overlap and were connected to the same electrode. Before measuring, an electrode test was carried out to examine if the contact between the cable, the electrodes and the ground was adequate, and that all electrodes were properly connected to the cable. This is done to prevent incorrect readings. After the electrode test, measurements were initiated with a long protocol (GRAD4LX8) and then a short protocol (GRAD4S8). The long protocol used all four cables, but only every other electrode, obtaining information to a greater depth. The short protocol collected data from a shallow depth by using every electrode, but only the two mid cables (the other two cables are not used in this protocol).

After measuring the two protocols, the instrument was moved one step upwards in the configuration, and the first cable (1) was disconnected and moved up in front. As a result, the instrument was continuously in a centre position. This measuring technique is called a roll-along (Fig. 15) and was used through out the measurements of the profiles.

The following equipment was used during the resistivity survey: ABEM terrameter SAS4000, electrode selector ES10-64C, electrode cables, electrodes of steel, cable jumpers, cable connectors and 12 Volt DC batteries.

3.3.1 Topography measurements and calculation

To measure the topography two 1 m sticks, 20 m of string, a hanging compass (inclinometer), a GPS and a handhold compass was used. Between the two 1 m sticks the 20 m string was rigged. Depending on the morphology of the ground, the string was regulated to cover the difference in height. The hanging compass was positioned in the middle of the string and the angel was read in degrees. The string was always tighten at a fixed height above ground. The hand held compass was used to get the right direction, and a GPS point was taken every 100 m. The elevation data was calculated in computer software Excel by the equation 1.5 to get the height difference (x);

$$x = a + \left(\sin\left(b\right) \cdot c\right) \qquad (1.5)$$

a = the value of the previous height measuring point
b = angel in radian
c = distance from previous height measuring point

To get the correct elevation above sea level (m.a.l.s) a starting point (y_{start}) and an ending point (y_{end_corr}) was collected from the digital elevation model in ArcGIS. Due to the major difference in elevation between starting point and ending point in Long profile 1_1 and 1_2, the topography had to be corrected (Fig. 16). This correction was carried out by recalculate the wrongly calculated elevation (y_{false}) in every measure point, using equation 1.6

$$y_{corr} = y_{false} - \left(y_{end\_false} - y_{end\_corr} \cdot \frac{x_1 - x_{start}}{x_{end} - x_{start}} \right) \quad (1.6)$$

x_{start} = starting point of the profile
x_1 = distance to the false hight.
X_{end} = ending point of the profile
y_{start} = correct m.a.s.l at starting point
y_{false} = wrong calculated hight at x1
y_{end_false} = wrong calculated hight in ending point
y_{end_corr} = correct m.a.s.l at ending point

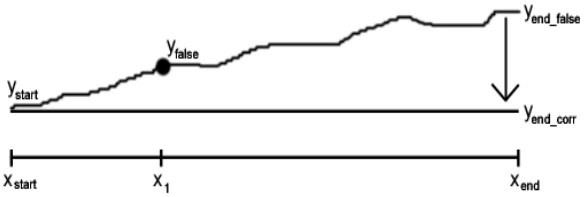

Fig. 16 Principles for recalculation of excessive height values in m.a.s.l.

3.4 Data processing

The field data was downloaded in to a computer through a serial cable connecting the computer and the Terrameter. The Terrameter was set to communication mode and the data was imported to the utility software for SAS4000, where the data were converted to a *.DAT file (Loke 2009). To identify and select bad data points, a pseudo section is useful that illustrate the measured apparent resistivity for supplementary interpretations. A bad data point is generally standing anomalously high or low values. The *.DAT file was opened in the modeling software Res2div to remove the bad data points. Bad data points are categorized in two broad groups, it can be either systematic or random noise. Systematic noise is generally caused by a failure of some sort during the survey (e.g. breaks in the cable, poor ground contact at an electrode), and the readings does not represent a true resistivity measurement (Loke 2009).

The problem with random noise is that it may not be readily explained, and as it might prove impractical to remove manually, specialized computer software can be of great assistance (Loke 2009).

The Res2div program creates a model by comparing the calculated apparent resistivity data with the measured values from the survey (Loke 2004). Every new round is called iteration and is presented in a pseudo section. Normally iterations are preformed 3-7 times to get a useful result. This whole process is called inversion (Jeppsson 2004). There are two types of inversion; robust inversion (l1-norm) and least squares inversion (l2-norm). The robust inversion is used in this study, which generally gives best result where the subsurface geology has sharp boundaries. The least-squares inversion is suitable for environments with a smooth variation in resistivity. The inversion in Res2div results in a deep section model of the resistivity distribution in the ground (Loke 2009). This deep section model was finally presented with depth interval, resistivity intervals, ect. in a program called Erigraph. Erigraph is mainly designed to facilitate graphical presentation of CVES (2D electrical imaging) data (Dahlin 2007). Data from a 2D imaging survey is normally plotted in pseudosection that gives a very approximate picture of the true surface resistivity distribution in a model section (Loke 2009). The data points are plotted in a diagram, where the length axis is represented by the distance along the surveying line and the depth axis for the electrode separation (Dahlin 1993).

Since the shape of the contours depends on the type of configuration and the true subsurface resistivity, the pseudosection gives a distorted picture of the subsurface (Loke 2009) as the apparent resistivity reflects the variation of resistivity in the ground in a qualitative manner. Hence, when interpreting the data, the approximate structure and depth of layer can, be estimated (Dahlin 1993).

3.5 Ground surveying methods

Ground surveying was performed on samples collected along the profiles (Table 1). Samples were collected at an even distance (~100m). Each sample weighed ~500 -600g and due to the problem with transportation, the number of samples had to be divided into halves (27 samples). In addition, five rock samples were collected, three in Area 1and two in Area 2.

The location of the boreholes were decided based on access. The consolidated nature of the ground and too loose material were parameters that also played a role in the decision. In too consolidated ground it was not possible to penetrate the ground with the handheld auger, and in too loose ground the material just kept falling in and filled up the borehole. The grain size analysis was preformed to get information about the grain size and for correlation with the resistivity data. The calcium carbonate was conducted to determine if some material could be of marine origin. Loss on ignition analyses (LOI) was preformed to determine the amount of organic matter in the samples. The discharge measurements were conduct to determine the recharge and infiltration of the surface water.

3.5.1 Grain size analysis

3.5.1.1 Sieving

All samples were dried at 105°C over night. The wet sieving was performed using 200 g of material of the well sorted grain size. The sieving of samples of the coarser fraction was performed with 300 g. Each sample was covered (~5 cm above sample surface) with 0.05 M sodium pyrophosphate ($Na_4P_2O_7$), saturating the sample until all aggregates were dissolved.

This procedure was followed by sieving through a 0.063 mm mesh. The washed samples were placed in a bowl, after 30 sec the sample was decanted and dried at 105°C over night.

The dry samples were placed in the sieve staple with the range of 22.4 – 0.063 mm. The sieve staple was put in the shaking machine for 15 min, after which all fractions were weighted and quantified according to Ambrosiani (1995).

3.5.1.2 Hydrometer analysis

Samples containing a 0.063 mm fraction that was >10 % were analyzed in a hydrometer. Theses samples were weighed and all particles > 2 mm were sorted out with the help of a sieve with a mesh of 2 mm. Remaining aggregates were crushed with a pestle and put in a 1000 ml cylinder, together with 100 ml 0.05 M sodium pyrophosphate ($Na_4P_2O_7$) and 300 ml distilled water. On top of the cylinder a cap of para film was placed and the cylinder was put in a cradle for 15 min.

Distilled water was put in the cylinder up to 990 ml. The sediment was mixed with a agitator for 1 min. After 1 min the agitator was pulled out and cleaned with distilled water. Simultaneously the time was started and a hydrometer was placed in the plastic cylinder. The hydrometer was read in time intervals of 0.5, 1, 2, 5, 10, 20, 50, 100, 200, 400 min and 1 day after the timer was started. The mixing process for each sample was repeated for the initial six readings (0.5, 2, 5, 10, 20 min) to determine possible standard deviation. All data were processed in Microsoft Office Excel 2003 to create the fraction curve. The fraction curve was used for calculate the hydraulic conductivity with Hazen's lay (equation 1.7).

Sample	**Grain size analysis**		**Loss on ignition**	**Calcium carbonate content**	**Mineral content**
	Sieving	**Hydrometer**			
Area 1					
1_1a	X			X	
1_1c	X			X	X
1_1e	X			X	
1_1g	X			X	
1_3b	X			X	
1_3c	X			X	
BH5a	X	X	X	X	
BH5b	X	X	X	X	
BH5c	X			X	
BH5d	X			X	
BH5e	X			X	
Area 2					
2_1b	X			X	X
2_1d			X	X	
2_1f	X		X	X	
2_1g	X	X	X	X	
2_2b			X	X	
2_2e	X	X	X	X	
2_3a	X	X	X	X	
2_3b	X			X	
2_3c	X			X	
2_3d	X			X	X
Gravel Pit	X	X		X	X
BH6a	X	X		X	
BH6b	X	X		X	
BH6c	X			X	
BH6d	X			X	
BH6e	X			X	

Table 1 Guide over analyses preformed on samples in Area 1 and 2.

$$K = 0.01157 \cdot d_{10}^{2}$$

(m/s) only when

$$\frac{d_{60}}{d_{10}} < 5 \qquad (1.7)$$

3.5.1.3 Data processing

The data from the grain size analysis was processed in the file KORNSTORLEK in data software program Microsoft Office Excel 2003. In Excel the weigh of the grain size was put in, producing a grain size curve. The grain size was determined according to *Kompendium i Jordartsanalys- laboratorieanvisningar* (Ambrosiania 1995) depending on the distribution graphs and the calculated percentage.

3.5.2 Calcium carbonate content

The calcium carbonate ($CaCO_3$) content was tested by a milling test (Ambrosiani 1995), which was performed on all samples. Approximately a teaspoon of every sample was put in a small ceramic cup. The samples were moistened with water and then some drops of 10% hydrochloric acid (HCl), if the sample contains $CaCO_3$ the sample will mill. The content of $CaCO_3$ can be estimated according to Table 2.

Approximate amount of $CaCo_3$	Milling (content of calcium carbonate)
≤ 0.5%	Non
0.5-1%	Extremely weak
1-3%	Weak
3-5%	Strong but not sustained
>5%	Strong and sustained

Table 2 The approximate amount of $CaCO_3$ in relation to the amount of carbon dioxide development (Ambrosiani 1995).

3.5.3 Mineral content

To determine the mineral content and get information of the origin of fluvial deposit five samples were analyzed, one in Area 1 and four in Area 2. Several mineral analyses were preformed in Area 2 due to larger variation. The mineral fraction was 2 mm and was extracted from the sample with a mesh. The particles were then analyzed under microscope and divided in 5 different groups: quartz, bedrock fragments, volcanic bedrock, sandstone and secondary concretions. To separate the quartz from the bedrock fragments the following criteria were use: 1) quartz should be clean and have no particles of other minerals, 2) bedrock fragments were all minerals containing feldspar and all combinations of feldspar and quartz.

3.5.4 Loss on ignition

Loss on ignition (LOI) was conducted on samples that indicated high value of organic material. Ceramic crucibles were dried in the oven over night at 105 °C, cooled in a desiccator and weighed. 4-5 g of sample was pulverized and placed in the crucibles and dried at 105 °C for one hour. The sample were cooled in the desiccator and weighed on a scale with a three decimal accuracy. The sample was then put in a cold oven to

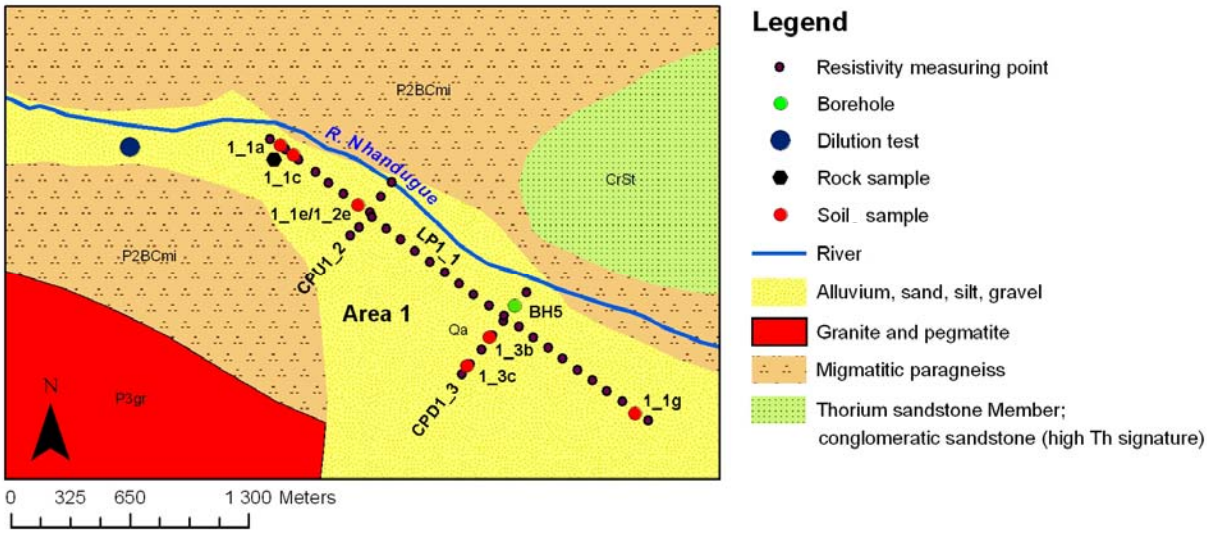

Fig. 17 Overview of the sample location in Area 1. Due to natural variations in the position of the Nhandugue River with season and between the years, the map shows a mean position of the river. Therefore a slight inaccuracy occurs in the location of the resistivity profiles in relation to the river as it was during the fieldwork.

prevent incomplete combustion and the temperature was slowly increased to 550 °C. The sample was placed in a desiccator to cool. The combusted sample was weighted. The difference in weight before and after the combustion was calculated. By dividing the weight difference with the weight of the dried sample, multiplied by 100, LOI was calculated in percentages.

3.5.5 Discharge survey

The discharge in Area 1 was studied on top of the outcrop in three channels, the main channel and two smaller channels, to see the initial water flow. In Area 2 the discharge was studied in the main channel.

The discharge in Area 1 and 2 was measured by a dilution of 500 g normal table salt (NaCl) that was dissolved in a 20 l bucket of floodwater. The temperature and the electrical conductivity were noted both in the bucket and in the river. The bucket with water was directly poured in to the river water and the electrical conductivity with unit µS/cm (micro simens per cm) was measured 10 m downstream in approximate 1 seconds interval using an HQ40d Dual-Input Multiparameter Meter Configuration. The discharge is given by the equation 1.8:

$$Q = \frac{M \cdot EC_1}{\int EC} \qquad (1.8)$$

EC = electrical conduction in µS/cm downstream of the injection point.
M = the amount of used water (l)
EC_1 = electrical conductivity of the tracer solution (µS/cm).

The integral equals the area under the resulting graph, minus the base value. The measured value is multiplied with the time and the result has the unit micro siemens per centimeter over time (µS/cm·s). EC_1 is the electrical conductivity of the solution that consists of NaCl (modified from Steinbruch & Merkel 2008).

4 RESULTS

4.1 Geophysical surveying methods

4.1.1 Area 1

Area 1 consist of three profiles (Fig. 17), Long profile 1_1 (LP1_1) along the river channel, and two short profiles, Cross profile upstream 1_2 (CPU1_2) and Cross profile downstream 1_3 (CPD1_3). The electrode separation was 5 m, giving a penetration depth of approximately 60-70 m. The coordinates and length of the tree profiles are presented in Table 3.

The resistivity and IP profile of LP1_1 is presented in Fig. 18 and Appendix 4a, while CPU1_2 is presented in Fig. 19 and Appendix 4b and CPD1_3 is presented in Fig. 20 and Appendix 4c. LP1_1 is 2585 m long and the mean residual is 4.0 % for resistivity and 20.1 % for IP, with 5 iterations. The profile starts at the contact zone between the outcrop and the river channel (~105 m.a.s.l.), and ends on the other side of the river (~95 m.a.s.l.).

CPU1_2 is 400 m long and the mean residual is 5.2 % for resistivity and 16.0 % for IP, with 5 iterations. This profile begins on the NE side of the channel (~120 m.a.s.l.) and is terminated at the border of the cemetery located at the other side of the channel (~110 m.a.s.l.). Furthermore, it crosses LP1_1 at approximately 700 m (see arrow in Fig. 18 and 19).

CPD1_3 is 575 m long and the mean residual is 6.4 % for resistivity and 20.4 % for IP, with 6 iterations. The profile starts off in a field of grass and crops on the NE side of the channel, and ends in the vegetation on the SW side of the channel. LP1_1 is crossed at approximately 1600 m (see arrow in Fig. 18 and 20).

Profile name	Coordinates	Length (m)
Long profile 1_1 (LP1_1)	79.58326°N, 63.9999°E / 79.56822°N, 64.1995°E	2585
Cross profile upstream 1_2 (CPU1_2)	79.58089°N, 64.0661°E / 79.57799°N, 64.0436°E	400
Cross profile downstream 1_3 (CPD1_3)	79.57486°N, 64.1400°E / 79.57040°N, 64.1044°E	575

Table 3 The coordinates and length of the profiles in Area 1.

4.1.1.1 Resistivity

In LP1_1 (Fig. 18) four units are identified:

- The top unit (1) is ~5-10 m thick, with medium resistivity (270-600 Ωm).
- Unit two (2) constitutes the initial ~900 m of the profile, from the NW to SE, and is ~60 m thick with high resistivity (600-3000 Ωm).
- Unit three (3) is located in the middle of the profile; it is ~600 m long (from 900 to 1500 m), ~60 m thick, and has a medium resistivity (120-600 Ωm). This section underlies unit four (from 1500 to 1800 m), forming a wedge towards SE.
- Unit four (4) comprises the last ~1100 m of the profile (from 1500 to 2600 m) and have an average thickness of ~60 m, with low resistivity (2.2-25 Ωm). This section covers unit three from 1500 to 1800 m.

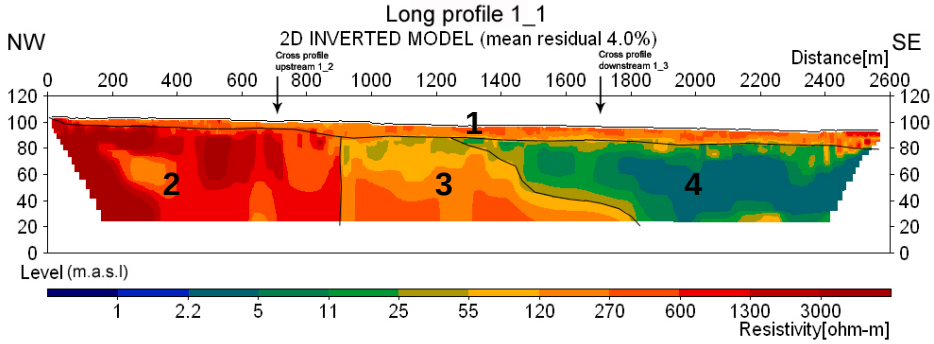

Fig. 18 Long profile 1_1 shows a thin top unit (1) and the three units below, 0 to ~900 m (2), ~900 to ~1500 m (3) and ~1500 to 2600 m (4), respectively.

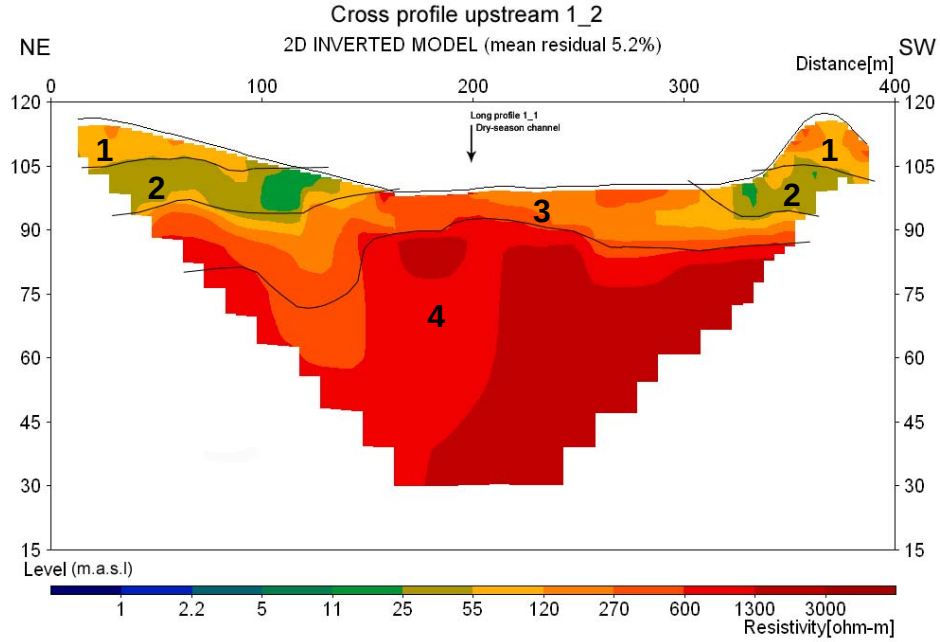

Fig. 19 Cross profile 1_2 shows four defined units (1-4), top unit (1), unit two (2), unit three (3) and unit four (4).

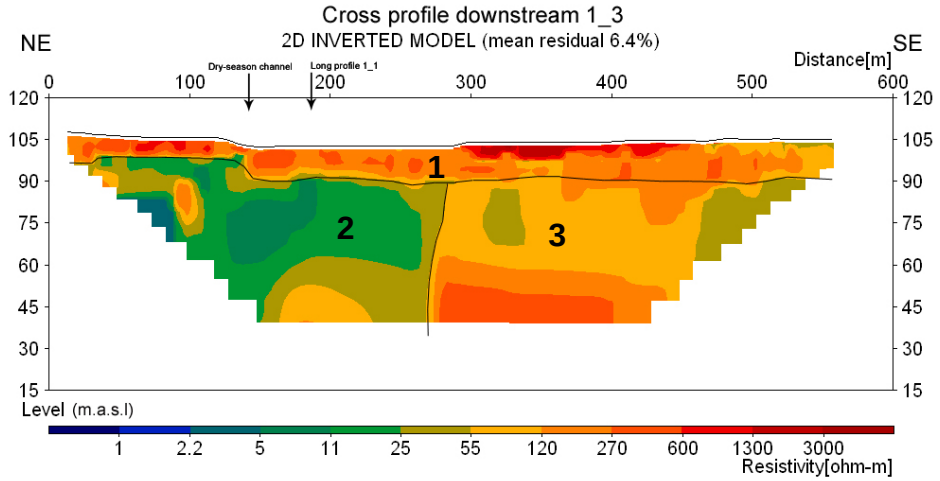

Fig. 20 Cross profile 1_3 shows a thin top unit (1) and two units below, 0 to ~300 m (2) and ~300 to 570 m (3), respectively.

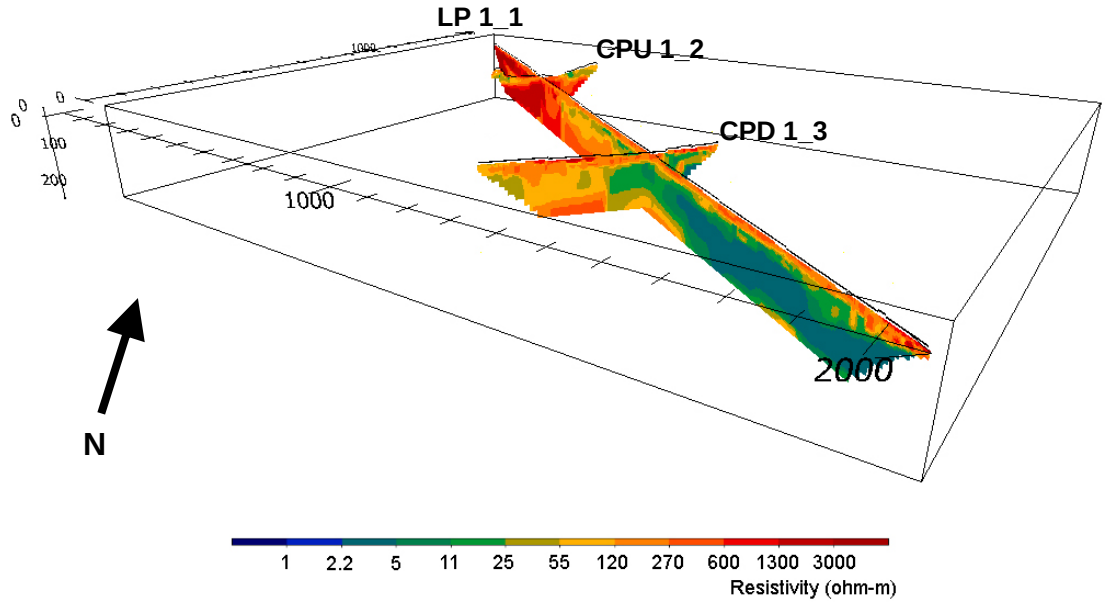

Fig. 21 3D-model of the resistivity for Area 1 showing profile LP1_1, and the two cross profiles CPU 1_2 and CPD1_3.

In CPU1_2 (Fig. 19) four units have been identified:

- The top unit (1) is ~15 m thick, with medium resistivity (120 Ωm). The areas from 0 to 100 m and 350 to 400 m along the profile are slightly elevated.
- Unit two (2) is ~15 m thick, with low resistivity (5-55 Ωm). This layer is marked in green in Fig. 19, and extend from 0 to 150 m and from 300 to 400 m along the profile.
- Unit three (3) is ~10 m thick, with medium to high resistivity (270-600 Ωm).
- Unit four (4) is ~50 m thick, with high resistivity (1300-3000 Ωm).

In CPD1_3 (Fig. 20) three units are identified:

- The top unit (1) is ~10-15 m thick, with medium to high resistivity (270-1300 Ωm).
- Unit two (2) represents the initial ~300 m of the profile and has an average depth of ~50 m, with low resistivity (5-55 Ωm).
- Unit three (3) corresponds to the final ~270 m of the profile (from 300 to 570) and is ~50 m thick with medium resistivity (55-270 Ωm).

In Fig. 21, all three profiles have been fitted together into a 3D-model.

4.1.1.2 Induced Polarization

LP1_1 has a chargeability between 7.9-22 mV/V, with the exception of two areas, at ~650-1200 m and ~1800-2600 m, that contain artifacts (36-70 mV/V) (Appendix 4a). CPU1_2 has a chargeability of 7.9-22 mV/V, with a minor artifacts (36-70 mV/V) at ~290 m (Appendix 4b). CPD1_3 has a chargeability of 7.9-22 mV/V, with a minor artifacts (42 mV/V) at ~340 m (Appendix 4c).

All profiles have a high residual (16-20.4%) due to the generally poor contact between electrodes, and when normalizing the chargeability only useless noise was produced.

4.1.1.3 Ground surveying results

All results from grain size analyses, determination of hydraulic conductivity, calcium carbonate ($CaCO_3$) content and loss on ignition are presented in Table 4. The location of the samples are presented in Fig. 17.

Grain size analyses of the surface samples from the various profiles (1_1a, 1_1e/1_2e, 1_1g, 1_3b, 1_3c) have been classified as medium to coarse sand (Appendix 2), with the exception of surface sample 1_1c, which was classified as sandy gravel. The mineral analysis of sample 1_1c show that the main components are crystalline rock fragments (60 %), quartz fragments (36%) and sandstone particles (4%) (Fig. 22). The crystalline rock fragments consists of mixed minerals of biotite, feldspar (as microcline and plagioclase) and quartz.

Three rock samples, collected on each side of the outcrop where LP1_1 starts (Fig. 23 a-c), has a composition of plagioclase, biotite, quartz, amphibolite and kalifeldspar. The surfaces of the samples are generally weathered, grey in colour and with visible stripes.

In the southern direction of the outcrop, eye gneisses with clusters of 2-3 cm consisting of plagioclase and kalifeldspar are more prominent (Fig. 23a). The "eyes" can also have a more boudinage (cylinder-like) structure. The matrix consists mainly of biotite, quartz and plagioclase. The eye gneiss is rather porous and may have some iron precipitation. In the northern

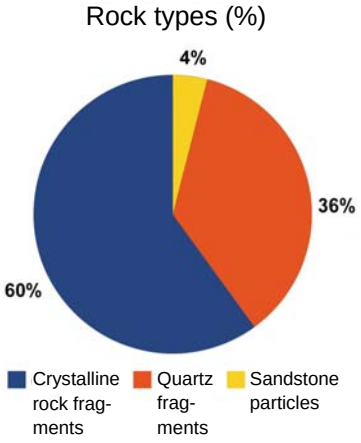

Fig. 22 Pie chart displays the mineral content of sample 1_1c in percent (%). Three rock types are represented: crystalline rock fragments (60%), quartz fragments (36%) and sandstone particles (4%).

direction, ordinary gneiss of the same mineral composition is generally present (Fig. 23b).

A ~1 m wide dike has been identified within the outcrop, with an N-W direction, a dip of ~90° and with a sharp boundary towards the surrounding bedrock. The dike is fractured, with water flowing from the dike into the channel. The field observation shows that the whole area has a high concentration of sinistral movements (bend to the left) (Fig. 23c).

The hydraulic conductivity of the samples ranges from $0.56 \cdot 10^{-2}$ to $3.70 \cdot 10^{-2}$ m/s. The lowest value is recorded in sample 1_1e/1_2e, while the highest were found in sample 1_1c. All samples contain ≤ 0.5 % amounts of $CaCO_3$ (Table 4).

Borehole 5 (Fig. 24) is 2.5 m deep, consisting of sand with alternate grain size. The top 0.35 m is dark brown, partly silty clayey sand with some organic matter, while the following 0.89 m (0.35-1.24 m) is brown partly silty gravelly sand that is coarsening downwards. The interval from 1.24 m to 2.05 m is represented by dark orange sand with a coarse fraction, which changes to a homogenous medium to coarse sand of the same colour from 2.05 m to 2.25. The final 0.25 m of Borehole 5 (2.25-2.50 m) consist of gravelly sand of matching dark orange colour (Fig 24). Sample BH5a constitute the first 35 cm of the borehole, and contains ~4.93 % organic material. Sample BH5b constitute the layer between 0.35-1.24 m, and contain ~2.35 % organic matter.

4.1.1.4 Discharge measurements

The results of the discharge measurements for the main channel and the parametric data are presented in the Fig. 25. The survey was performed at the 14th of August 2009 during the dry-season when no rainfall hade occurred in the area for month.

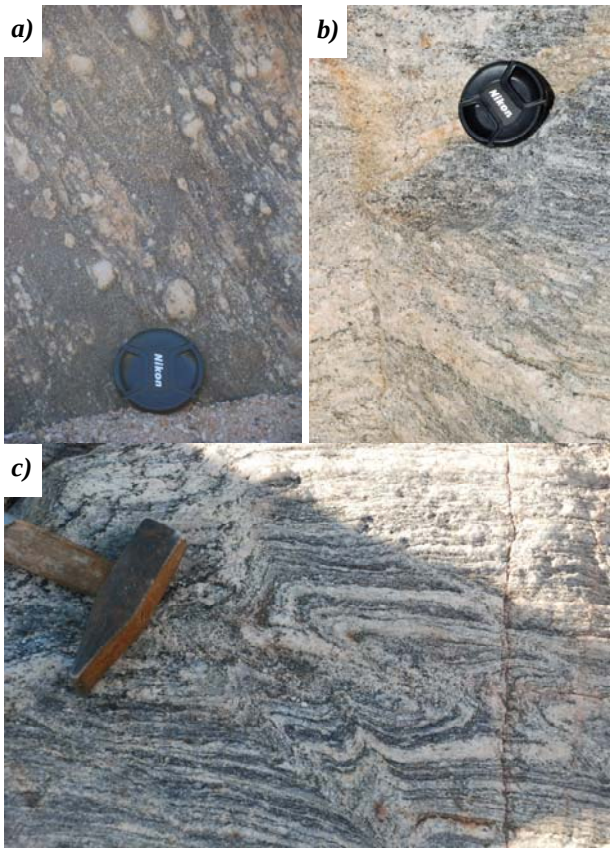

Fig. 23 a) Eye gneisses with clusters of 2-3 cm consisting of plagioclase and kalifeldspar. Located at 79.58212°N, 64.0025°E b) "Normal" gneiss. Located at 79.58300°N, 64.0073°E c) The whole area has a high concentration of sinistral movements (bend to the left).

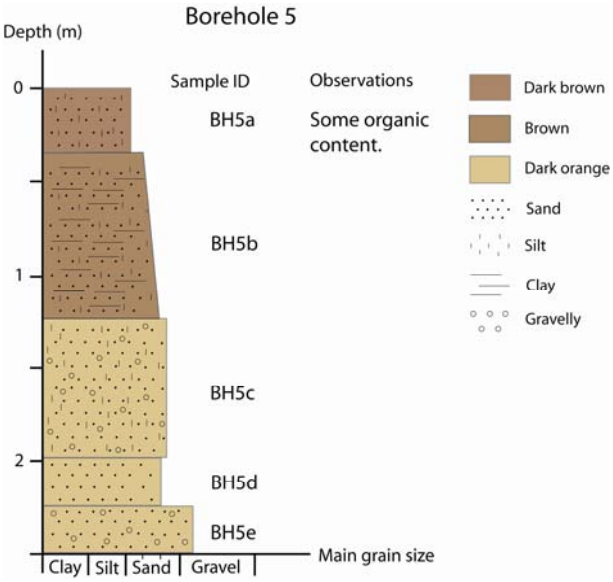

Deepth (m)	Colour	Sample number
0.00 - 0.35	Dark brown	BH5a
0.35 - 1.24	Medium brown	BH5b
1.24 - 2.05	Dark orange	BH5c
2.05 - 2.25	Dark orange	BH5d
2.25 - 2.5	Dark orange	BH5e

Fig. 24 Log of borehole 5 in Area 1 displaying the type of soils, grain sizes, location of soil samples and field observations.

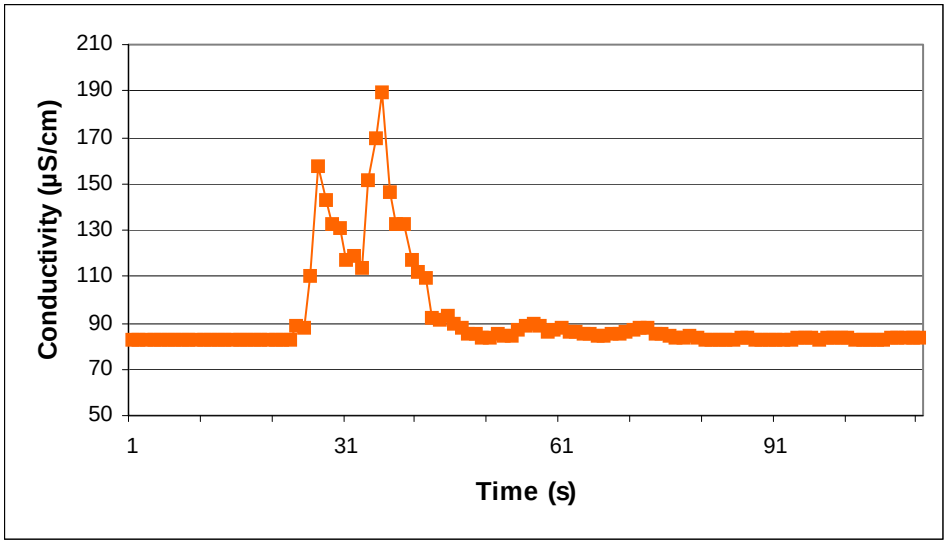

Fig. 25 Graph showing conductivity over time for the main dry-season channel. For location see Fig. 17.

Table showing value of EC_1 (electrical conductivity of the tracer (NaCl solution), ∫EC (integral of the measured EC) and calculated Q (discharge) for the main channel.

NaCl solution, EC_1 (µS/cm)	Electrical conductivity, ∫EC (µS/cm · s)	Discharge, Q (l/s)
30100	1265	476

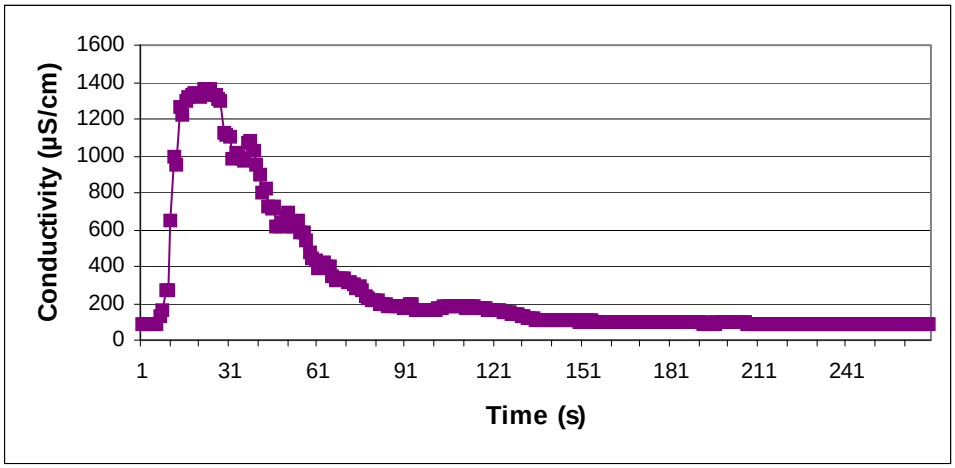

Fig. 26 Graph showing conductivity over time for the small dry-season channel. For location see Fig. 17.

Table showing value of EC_1 (electrical conductivity of the tracer (NaCl solution), ∫EC (integral of the measured EC) and calculated Q (discharge)

NaCl solution, EC_1 (µS/cm)	Electrical conductivity, ∫EC (µS/cm · s)	Discharge, Q (l/s)
30800	6838	89

Mixing 500 g salt in 20 l water provided a tracer solution with a value of 30100 µS/cm. The measured electrical conductivity (EC) is present as micro Siemens over time (µS/cm · s) due to the calculation of the integral. The integral of the measured EC was calculated to 1265.40 µS/cm · s, and by using equation 1.9 the discharge (Q) was calculated to 476 l/s. The result of the discharge measurements and the data for the small channel located in the middle of the study area is presented in Fig. 26. The tracer solution had a value of 30800 µS/cm. The integral of the measured EC was calculated to 6837.90 µS/cm · s, and Q was calculated to 89 l/s. Collectively, the main channel and the small channel produce a discharge of 565 l/s.

4.1.2 Area 2

Area 2 consist of tree profiles (Fig. 30), Long profile 2_1 (LP2_1) along the river channel, and two short profiles, Cross profile upstream 2_2 (CPU2_2) and Cross profile downstream 2_3 (CPD2_3). The electrode separation was 5 m, giving a penetration depth of approximately 60-70 m. The coordinates and length of the three profiles are presented in Table 5.

The resistivity and IP profile of LP2_1 are presented in Fig. 27 and Appendix 6a, while CPU2_2 and CPD2_3 are presented in Fig. 28 and 29 and Appendix 6b and 6c, respectively. LP2_1 is 2500 m long and the mean residual is 7.1% for resistivity and 45.1% for IP,

Samples	Grain size analysis		Approximate amount of $CaCo_3$ (%)	Loss on ignition (%)
	Grain size	Hydraulic conductivity (m/s) · 10^{-2}		
1_1a	Sand (Medium to coarse)	0.278	≤ 0.50	
1_1c	Sandy gravel	0.74	≤ 0.50	
1_1e/1_2e	Sand (Medium to coarse)	0.078	≤ 0.50	
1_1g	Sand (Medium)	0.037	≤ 0.50	
1_3b	Sand (Medium to coarse)	0.56	≤ 0.50	
1_3c	Sand (Medium to coarse)	0.56	≤ 0.50	
BH5a	Silty sand		≤ 0.50	4.93
BH5b	Partly silty clayey sand		≤ 0.50	2.35
BH5c	Partly silty gravelly sand		≤ 0.50	
BH5d	Sand (Coarse)		≤ 0.50	
BH5e	Gravelly sand		≤ 0.50	

Table 4 Chart showing the results of grain size analysis, hydraulic conductivity, calcium carbon ($CaCO_3$) content, loss on ignition and discharge.

with 7 iterations. The profile starts in the water (~90 m.a.s.l.), crosses the river and ends on a field with crops (~87 m.a.s.l).

CPU2_2 is 900 m long and the mean residual is 5.8 % for resistivity and 37.5 % for IP, with 3 iterations. The profile is initiated at the valley side (~98 m.a.s.l) and ends in the river channel (~90 m.a.s.l), and it crosses the long profile perpendicular at around 200 m (see arrow in Fig. 27 and 28).

The CPD2_3 is 900 m long and the mean residual is 5.2 % for resistivity and 22.0 % for IP, with 6 iterations. This profile starts very close to a graveled road (~87 m.a.s.l), crosses the river channel and ends on the other side (90 m.a.s.l.). It crosses the long profile perpendicular at around 1850 m (see arrow in Fig. 27 and 29).

Profile name	Coordinates	Length (m)
Long profile 2_1 (LP2_1)	79.56539°N, 64.4979°E / 79.55751°N, 64.7228°E	2500
Cross profile upstream 2_2 (CPU2_2)	79.57218°N, 64.5309°E / 79.56345°N, 64.5162°E	900
Cross profile downstream 2_3 (CPD2_3)	79.56204°N, 64.6809°E / 79.55361°N, 64.6560°E	900

Table 5 The coordinates and length of the profiles in Area 2.

4.1.2.1 Resistivity

In LP2_1 (Fig. 27) four resistivity units have been identified:

- The top unit (1) is ~5-15 m, with high resistivity (330-1400 Ωm).
- Unit two (2) is ~5-10 m thick and discontinuously, with low resistivity (8.8-37 Ωm).
- Unit three (3) is ~15-30 m thick, with medium resistivity (18-160 Ωm). This layer is thicker to the SE.
- Unit four (4) is ~15-40 m thick, with low resistivity (2.1-18 Ωm). The layer is thinner to the SE.

In the CPU2_2 (Fig. 28) four units have been identified:

- The top unit (1) is ~10 m thick, with a variation in resistivity between high to medium (330-1400 Ωm, 37-160 Ωm).
- Unit two (2) is ~5 m discontinuously, with low resistivity (8.8-37 Ωm).
- Unit three (3) is ~15 m thick and discontinuously, with medium resistivity (18-160 Ωm).
- Unit four (4) is ~45-65 m thick, with low resistivity (2.1-18 Ωm).

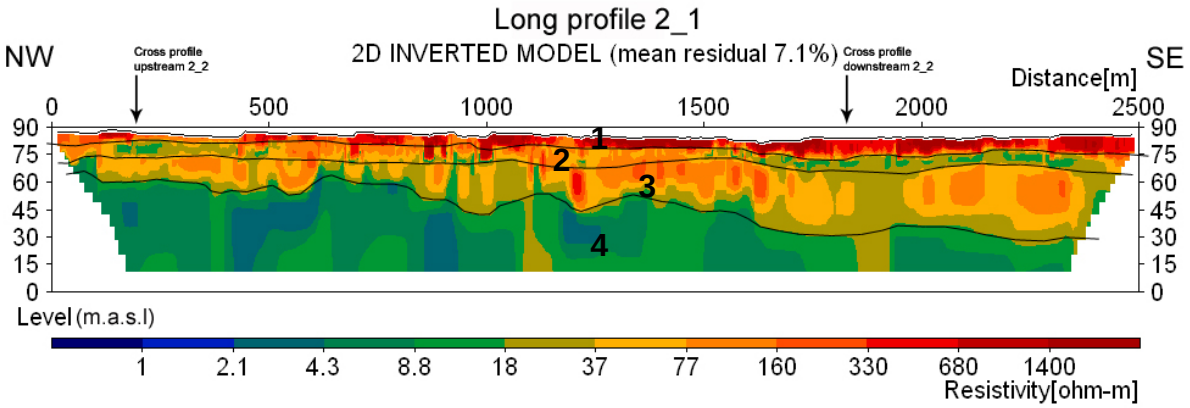

Fig. 27 Long profile 2_1 shows four defined units (1-4), top unit (1), unit two (2), unit three (3) and unit four (4).

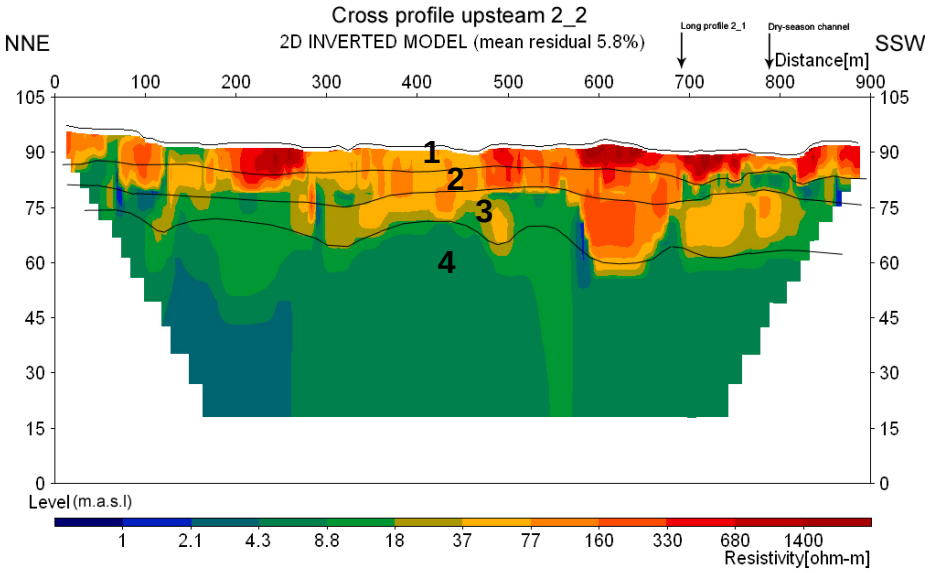

Fig. 28 Cross profile upstream 2_2 shows four defined units (1-4), top unit (1), unit two (2), unit three (3) and unit four (4).

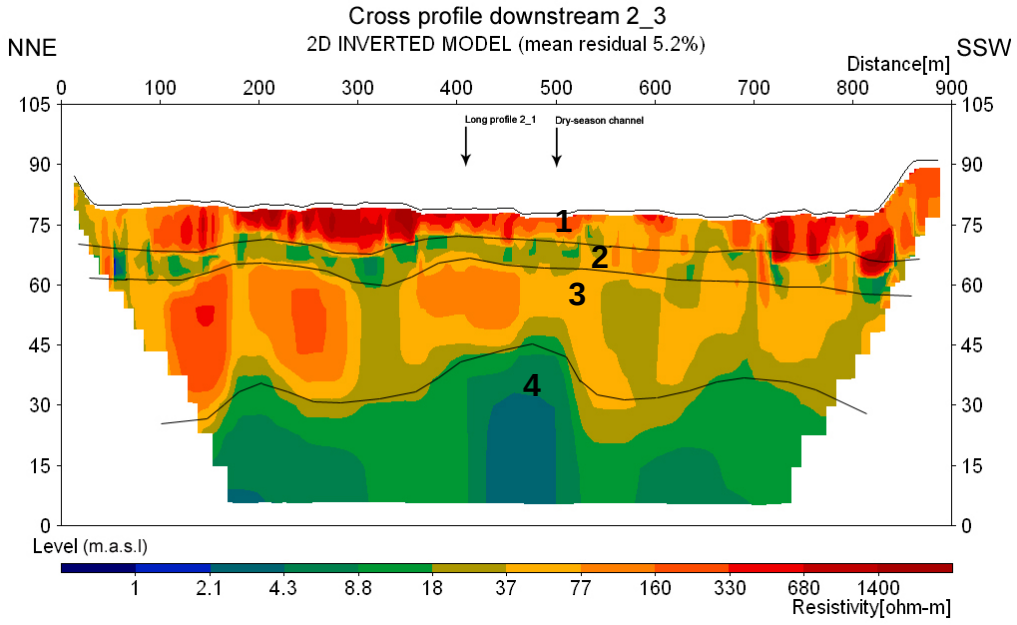

Fig. 29 Cross profile downstream 2_3 shows four defined units (1-4), top unit (1), unit two (2), unit three (3) and unit four (4).

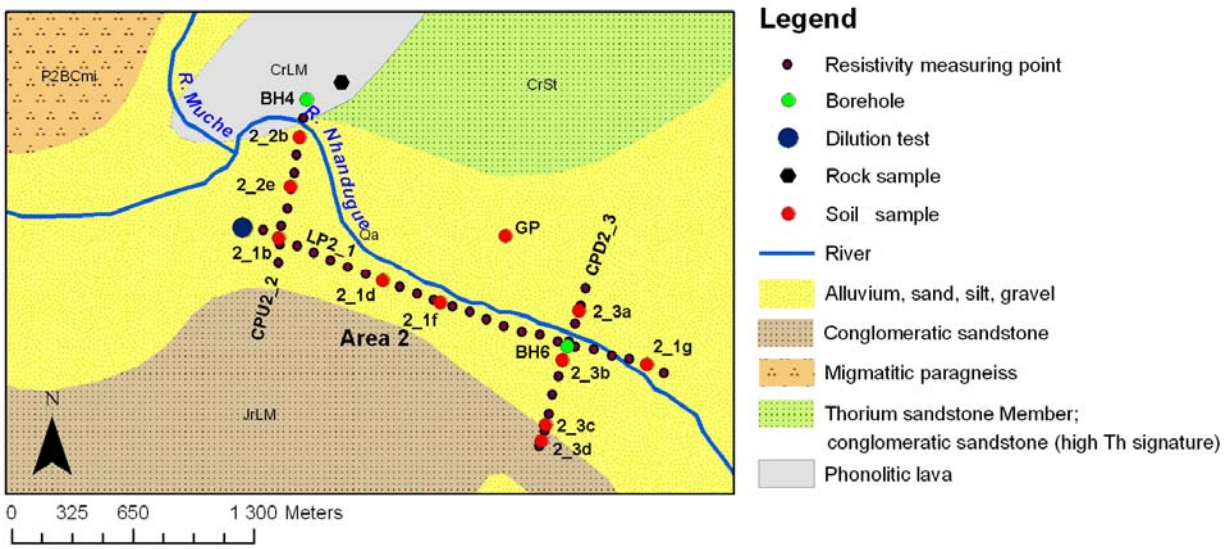

Fig. 30 Overview of the sample locations and position in Area 2. Due to natural variations in the position of the Nhandugue River with season and between the years, the map shows a mean position of the river. Therefore a slight inaccuracy occurs in the location of the resistivity profiles in relation to the river as it was during the fieldwork.

In the CPD2_3 (Fig. 29) four units have been identified:

- The top unit (1) is ~10-15 m thick, with high resistivity (330-1400 Ωm).
- Unit two (2) is ~10 m thick and discontinuously, with low resistivity (8.8-37 Ωm).
- Unit three (3) is ~20-30 m thick, with medium resistivity (18-160 Ωm).
- Unit four (4) is ~20-30 m thick, with low resistivity (2.1-18 Ωm).

In Fig. 31, all three profiles have been fitted together into a 3D-model.

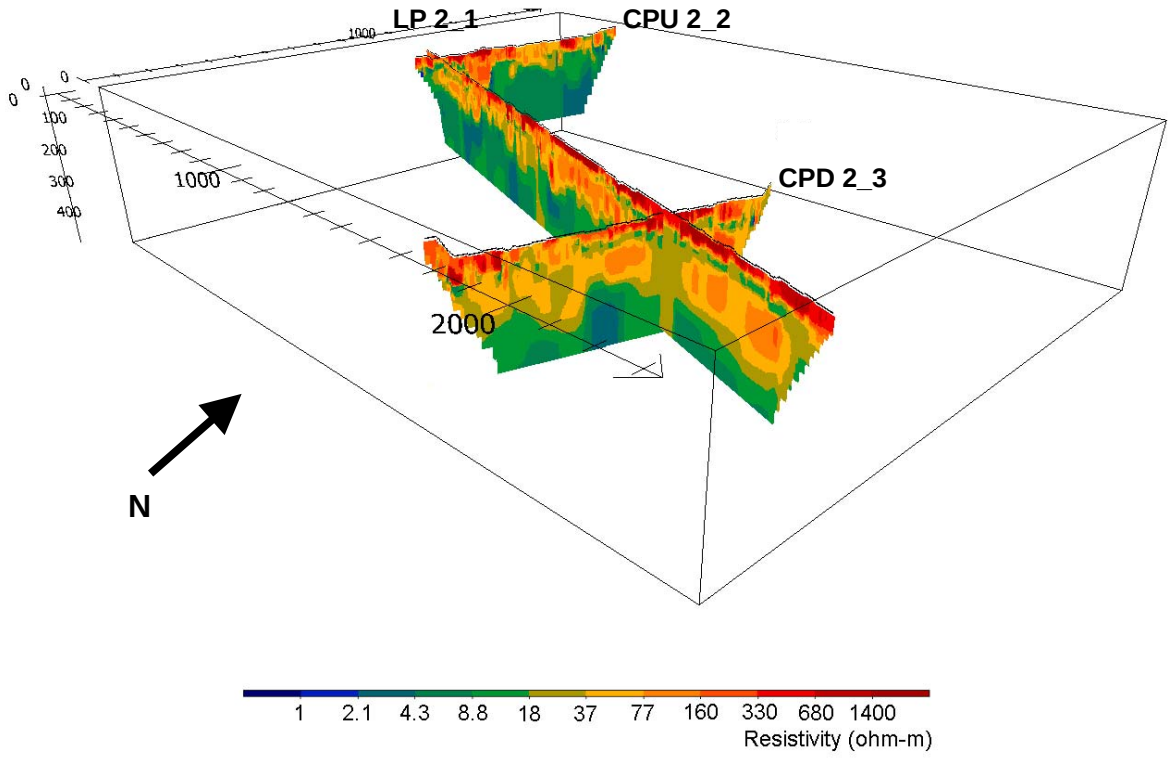

Fig. 31 3D-model of the resistivity for Area 2 showing profile LP2_1, and cross profiles CPU2_2 and CPD2_3.

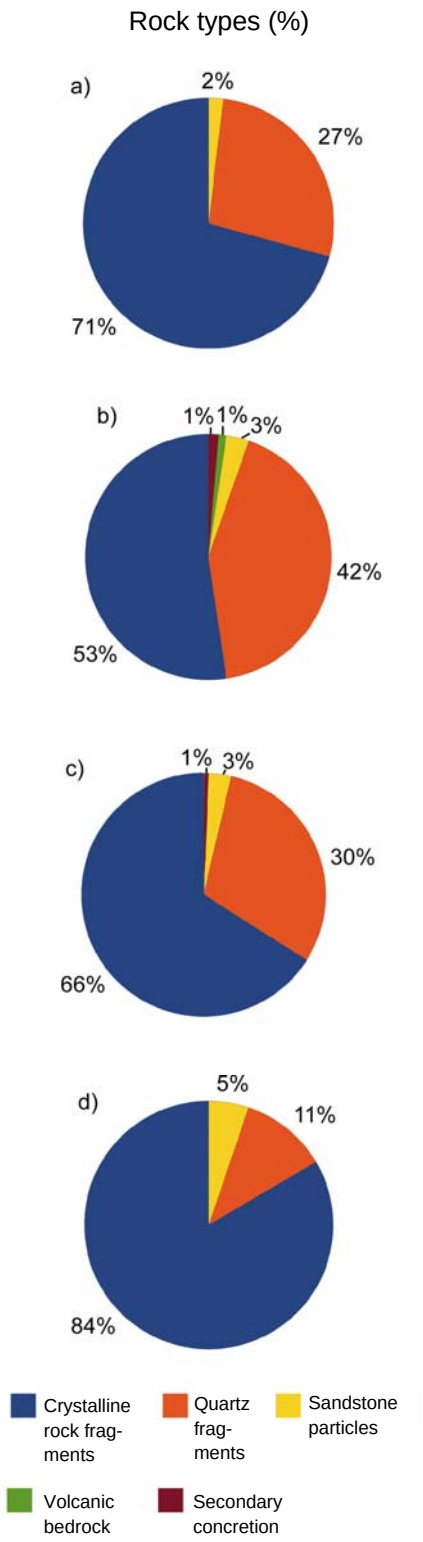

Fig. 32 Pie charts displaying the mineral composition of sample a) 2_ 1b, b) 2_3 d, c) Gravel Pit, and d) BH4b.

4.1.2.2 Induced Polarization

LP2_1 (Appendix 6a) has a chargeability between 7.9-22 mV/V, with artifacts between 36-70 mV/V. The artifacts are located across the entire profile. CPU2_2 (Appendix 6b) has a chargeability of 7.9-22 mV/V, with artifacts between 36-70 mV/V located in the NE. CPD2_3 (Appendix 6c) has chargeability between 7.9-22 mV/V, and no artifacts can be identified.

All profiles have a high residual (22-45.1%) which can be related to the commonly poor contact experienced between the electrodes. While the normalization of the chargeability did not provide any useful data for LP2_1 and CPU2_2, the process presented high values of 0.9-1 mS/m in the NNE region of CPD2_3 (see Fig. 44).

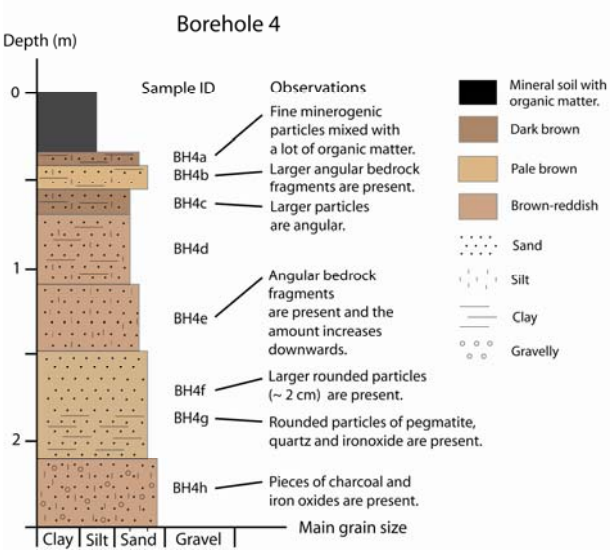

Deepth (m)	Colour	Sample number
0.00 - 0.35	Dark brown	
0.35 - 0.41	Dark brown	BH4a
0.41 - 0.55	Pale brown	BH4b
0.55 - 0.70	Dark brown	BH4c
0.70 - 1.10	Brown-reddish	BH4d
1.10 - 1.48	Brown-reddish	BH4e
1.48 - 2.10	Pale brown	BH4f (sample at 1.75m) + BH4g (sample at 1.80m)
2.10 - 2.52	Brown-reddish	BH4h

Fig. 33 Log of borehole 4 in Area 2 displaying type of soils, grain sizes, location of soil samples and field observations.

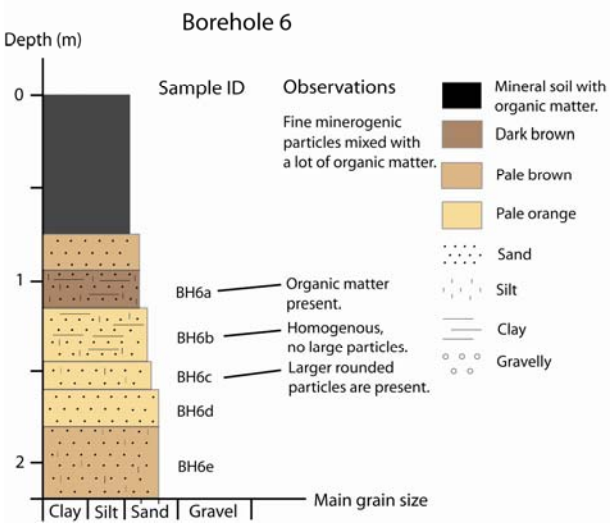

Deepth (m)	Colour	Sample number
0.00 - 0.75	Light brown	
0.75 - 0.95	Pale brown	
0.95 - 1.15	Dark brown	BH6a
1.15 - 1.45	Pale orange	BH6b
1.45 - 1.60	Pale orange	BH6c
1.60 - 1.80	Pale orange	BH6d
1.80 - 2.20	Pale brown	BH6e

Fig. 34 Log of borehole 6 in Area 2 displaying the type of soils, grain sizes, location of soil samples and field observations.

4.1.2.3 Ground surveying results

All results from grain size analyses, determination of hydraulic conductivity, calcium carbon ($CaCO_3$) content and loss on ignition are presented in Table 6. In Fig. 30, the location of the samples are presented.

Grain size analyses of the surface samples from the various profiles in Area 2 (2_1f, 2_2e, 2_3b, 2_3d) have been classified as sand in the fraction fine, medium and medium to coarse (Appendix 2). The surface samples 2_1d and 2_2b consist of mineral soil with organic matter. Sample 2_1b have been classified as gravelly sand, sample 2_1g is silty sand, sample 2_3a is clayey silty sand and sample 2_3c is sandy gravel.

The mineral analysis of sample 2_1b, 2_3d, Gravel Pit and BH4b (Fig. 32a-d) show that the main components are crystalline rock fragment (53-84%), quartz fragment (11-42%) and sandstone particles (2-5%). Sample 2_3d and Gravel Pit also consisting of secondary concretions (1%), and sample 2_3d contains 1% of volcanic bedrock. The crystalline fraction consists of mixed minerals of biotite, feldspar (as microcline and plagioclase) and quartz.

The two sedimentary rock samples were studied in a microscope. They are weathered and have a composition of quartz and feldspar, but differ in grain size between the rock samples.

Rock sample A has a homogeneous grain size of ~2 mm and is white to pink. It contains mostly feldspar and quartz, but is heavily eroded by clay weathering. It can be classified as a clay weathered fine-grained feldspar rich sandstone.

Rock sample B has a conglomeratic grain size of 0.5-1 cm and is white to reddish. It mostly contains feldspar and quartz, but is also profoundly eroded by clay weathering. It can be classified as a clay weath-

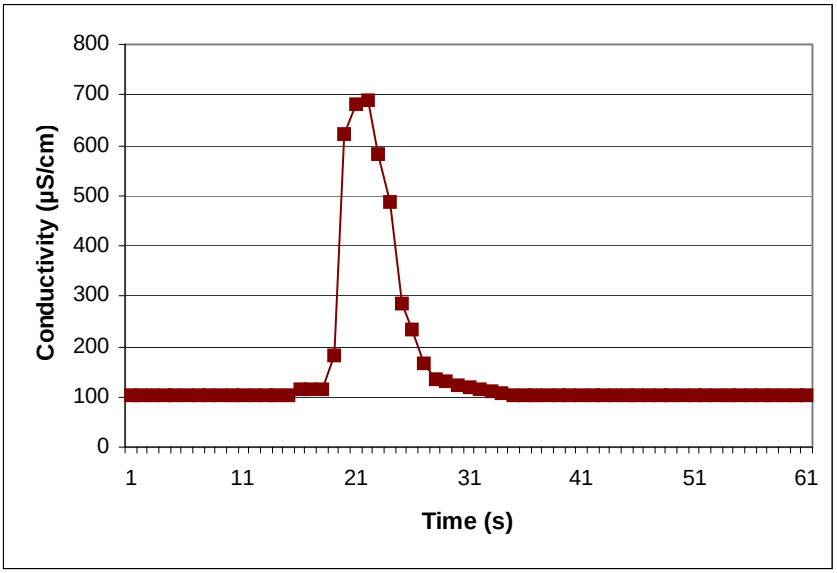

Fig. 35 Graph showing conductivity over time for the dry-season channel in Area 2. For location see Fig. 30 .

Table showing value of EC_1 (electrical conductivity of the tracer (NaCl solution), ∫EC (integral of the measured EC) and calculated Q (discharge) for the small channel.

NaCl solution, EC_1 (µS/cm)	Electrical conductivity, ∫EC (µS/cm · s)	Discharge, Q (L/s)
30900	2889	214

Samples	Grain size analysis		Approximate amount of $CaCo_3$ (%)	Loss on ignition (%)
	Grain size	**Hydraulic conductivity (m/s) · 10^{-2}**		
2_1b	Gravelly sand	0.185	≤ 0.50	
2_1d	Mineral soil with organic matter.		≤ 0.50	11.40
2_1f	Sand (Medium)	0.061	≤ 0.50	0.30
2_1g	Silty sand		≤ 0.50	3.00
2_2b	Mineral soil with organic matter.		≤ 0.50	10.70
2_2e	Sand (Fine)		≤ 0.50	1.70
2_3a	Clayey silty sand		≤ 0.50	3.30
2_3b	Sand (Medium)	0.038	≤ 0.50	
2_3c	Sandy gravel	0.245	≤ 0.50	
2_3d	Sand (Medium to coarse)	0.038	≤ 0.50	
Gravel Pit	Clayey gravelly sand		≤ 0.50	
BH4a	Silty clayey sand		≤ 0.50	3.80
BH4b	Silty clayey sand		≤ 0.50	3.20
BH4c	Silty clayey sand		≤ 0.50	3.40
BH4d	Silty clayey sand		≤ 0.50	
BH4e	Silty sand		≤ 0.50	
BH4f	Sand (Medium to coarse)		≤ 0.50	
BH4g	Clayey sand		≤ 0.50	
BH4h	Silty gravelly sand		≤ 0.50	
BH6a	Clayey silty sand		≤ 0.50	
BH6b	Partly silty clayey sand		≤ 0.50	
BH6c	Partly silty sand	0.022	≤ 0.50	
BH6d	Sand (Medium to coarse)	0.041	≤ 0.50	
BH6e	Partly silty sand	0.0296	≤ 0.50	

Table 6 Chart displaying the result of grain size analysis, hydraulic conductivity, calcium carbon ($CaCO_3$) content, loss on ignition and discharge.

ered coarse grained feldspar rich sandstone. The erosion is chemical and is probably kaolonite weathering.

The hydraulic conductivity of the samples (2_1b, 3_f, 2_3b, 2_3c,2_3d) ranges between 0.038 and $0.245 \cdot 10^{-2}$ m/s. The lowest value are recorded in sample 2_3b and 2_3d, while the highest value were found in sample 2_3c. All samples have ≤ 0.5 % amount of $CaCO_3$ (Table 6).

The loss on ignition of the samples (2_1d, 2_1f, 2_1g, 2_2b, 2_2e and 2_3a) has a sample range between 0.3-11.4 %. The lowest measurements were recorded in sample 2_1f, while the highest organic matter (>10%) is recorded in sample 2_1d and 2_2b.

Borehole 4 (Fig. 33) is 2.25 m deep. The top 0.35 m consist of dark brown fine mineralogical particles mixed with organic matter. The main grain size of the interval between 0.35-1.1 m is silty clayey sand, but the colour is alternating. In the top 0.35 to 0.41 m the sediment is dark brown, shifting to a pale brown in the next interval (0.41-0.55 m) followed by a patch of dark brown (0.55-0.7 m) that changes to a brown-reddish colour (0.7-1.10 m). The subsequent 1.10 to

1.48 m is represented by a brown reddish silty sand, followed by pale brown, medium to coarse sand that contain some clay further down (1.48-2.10 m). The last part (2.1-2.25 m) consist of a brown-reddish silty gravelly sand. The samples BH4a, BH4b and BH4c contain between 3.2-3.8% of organic material.

Borehole 6 (Fig. 34) is 2.2 m deep. The top 0.75 m consist of a light brown fine mineralogical particles mixed with a lot of organic matter, while the following 0.2 m (0.75-0.95 m) is pale brown medium to coarse sand, with organic matter present. The interval 0.95 to 1.15 m is dark brown clayey silty sand. The following 0.3 m (1.15-1.45 m) is pale orange, partly silty clayey homogeneous sand, not containing any large particles, while, the next interval 1.45-1.6 m is pale orange partly silty sand containing large rounded particles. 0.6-1.8 m is pale orange medium to coarse sand and the last 0.4 m (1.8-2.2 m) is pale brown partly silty sand. The hydraulic conductivity in BH6 (sample BH6c, BH6d and BH6e) is between $0.022\text{-}0.041 \cdot 10^{-2}$ m/s, with the lowest value in sample BH6c and the highest in sample BH6d.

4.1.2.4 Discharge measurements

The result and the parametric data of the discharge measurements are presented in Fig. 35. The survey was preformed at the 14th of August 2009 during the dry-season when no rainfall had occurred in the area in a month.

The measured electrical conductivity (EC) is present as micro Siemens over time (µS/cm · s). Mixing 500 g salt in 20 l water provides a tracer solution with a value of 30900 µS/cm. The integral of the measured EC was calculated to 2889 µS/cm · s, and by using Equation 1.8 the discharge (Q) was calculated to 214 l/s.

5 DISCUSSION AND INTERPRETATIONS

5.1 Area 1

LP1_1 (Fig. 36) contains all resistivity units also found in the two cross profiles, CPU 1_2 and CPD1_3. The red high resistivity unit (600-3000 Ωm) can be observed in the bottom unit of CPU1_2 (Fig. 37), but can not seen in CPD1_3 (Fig. 38). Reversibly, the yellow medium resistivity unit (120-600 Ωm) can not be seen in CPU1_2, but is visible as the SE unit in CPD1_3. The green/blue low resistivity unit (2.2-25 Ωm) in LP1_1 is not visible in CPU1_2, but is present in the NE unit of CPD1_3. The top of all the profiles has a medium resistivity of 270-600 Ωm. The river flanks consist of two units, a top unit with medium resistivity (120 Ωm) that covers a low resistivity unit (5-55 Ωm), which can not be seen in the other profiles. It is likely that the channel has cut through the two top units, consisting of sand with organic material and silt/clay, down to the level of the other profiles (~90 m.a.s.l). Furthermore, the upstream CPU1_2 profile starts at a higher elevation (~120 m.a.s.l) than the other profiles.

The resistivity measurements provide normally excellent data, however, the data can be interpreted in different ways due to the overlap in classifications of geological material.

The main interpretation of LP1_1 suggest that wet sand covers the gneiss which has been deformed during metamorphosis across the initial 900 m of the profile (NW-SE directions). Although the gneiss is mainly solid, fractures are present and has likely a NE-SW drainage direction along the faults. The faults are indicated by blue vertical lines in the profiles. Gneiss can also be observed at the bottom most layer of CPU1_2.

The middle section in LP1_1 also consist of gneiss with medium resistively (120-600 Ωm), but appears to be more fractured and weathered, possibly caused by the presence of water. This fractured gneiss can also be seen in the SE unit of CPD1_3.

The SE unit of LP1_1 is represented by saturated sandstone (2.2-25 Ωm) and may correspond to the Sena formation or/and the Lupata Group, according to the geological map (Appendix 1). This sandstone can also be observed in the NE unit of CPD1_3. The vertical and oblique resistivity boundaries between units probably represents faults in a NW-SE and N-S direction, respectively. The fault direction corresponds to the faults found in the geological map. The oblique boundary, linking the fractured gneiss of the middle section and the sandstone of the last section, may contain a minor fault that causes the fractured gneiss to dip towards the SE.

Together, LP1_1 and CPD1_3 confirm that sandstone is position on top of the fractured gneiss, and that it is dipping towards the SE.

The most plausible hypothesis explaining the formation of the faults at ~900 m, is that the gneiss was coved by sandstone prior to faulting. The gneiss was probably exposed to chemical and physical weathering by water, which result in its fractured nature. When the normal fault at ~900 m formed, it raised the level of the bedrock while lowering the sandstone. The sandstone on top was then eroded, exposing the gneiss. Hence, the shift from fractured gneiss (yellow) to sandstone (green) at ~1300 m is a sedimentation contact between the fractured gneiss and the sandstone.

A second, less likely, hypothesis is that the fault at ~900 m and ~1300 m were established during two separate events. As the fault at ~900m formed, it caused the fractured bedrock to sink, moving the more solid gneiss upward. When the fault at ~1300 m faulted, it forced the sandstone downward while the solid and fractured gneiss moved upwards. At this point in time, the fractured gneiss was located on top of the solid gneiss which in turn was covered by sandstone. The sandstone and gneiss was then eroded away by weather and water, creating a hiatus on top of the solid gneiss.

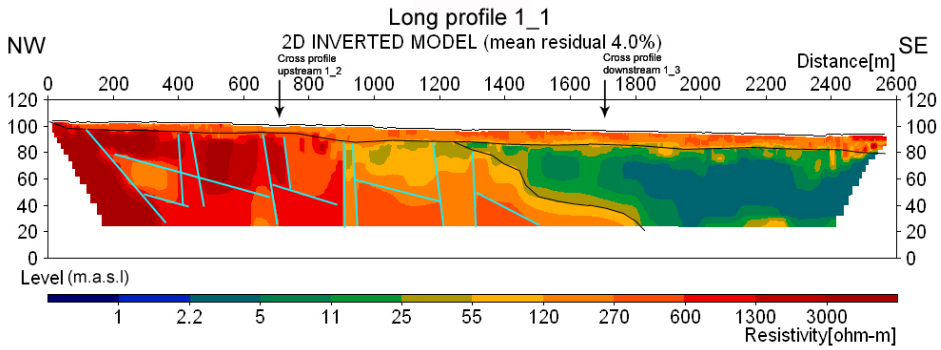

Fig. 36 Long profile 1_1 shows a thin top unit consisting of sand and the three units below, 0 to ~900 m consisting of gneiss with faults, ~900 to ~1500 m consisting of fractured gneiss and ~1500 to 2600 m consisting of sandstone. The blue lines represent possible faults.

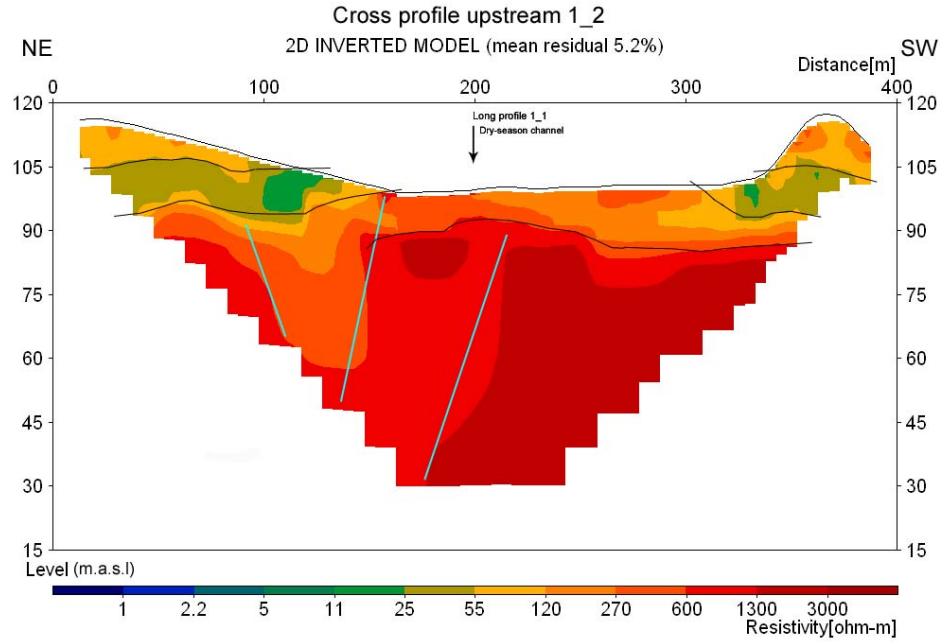

Fig. 37 Cross profile upstream 1_2 show the river flanks consisting of sand with organic material and silt/clay. The river channel is consisting of sand that cover the gneiss. The blue lines represent possible faults.

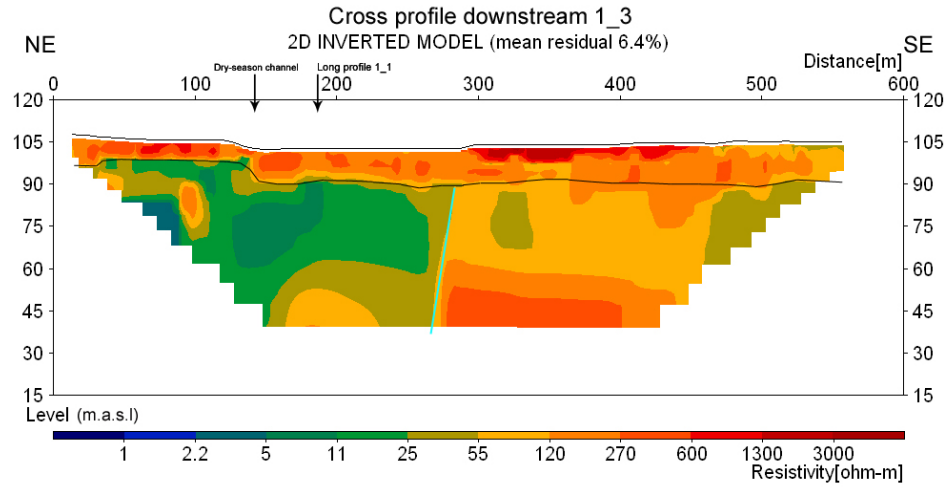

Fig. 38 Cross profile 1_3 reveal a top unit consisting of sand and two defined units below, 0 to ~300 m consisting of sandstone and ~300 to 570 m consisting of fractured gneiss, respectively. The blue lines represent possible faults.

A secondary interpretation of LP1_1 would imply that the first 100 m of the profile consist of solid gneiss that has probably been deformed during metamorphosis. The rest of the NW unit (red) is composed of coarser alluvial fill from erosion of the gneiss, including blocks of gneiss. The unit can also be observed in the bottom most layer of CPU1_2. It has numerous faults in the NW and the middle section.

The middle section of LP1_1 consists of alluvial sediments, fining outward and upward. Finer material can also be observed in the NE unit of CPD1_3, while alluvial sediment is predominate in the SE unit. The data from LP1_1 and CPD1_3, indicate that finer material is laying on top of the fractured bedrock, dipping towards the SE. Another fault divide the middle unit from the SE unit of LP1_1.

The main interpretation of the profile, and the primary hypothesis regarding the formation of the faults, appears to be the most likely explanation for the geological development of the area. The contact between the central and SE unit is gradual, and is not as sharp compared to the other fault in the same area. Hence, it seems reasonable that this probably constitute a sedimentation contact, and not a fault. Furthermore, the SE unit of LP1_1 has been interpreted as a sandstone, strongly indicated by the substantial thickness of this unit. In contrast, the equivalent deposition of fine grained material (silt and clay) would have required a prolonged period of low velocity water flow, which seems quite improbable in this sedimentary environment.

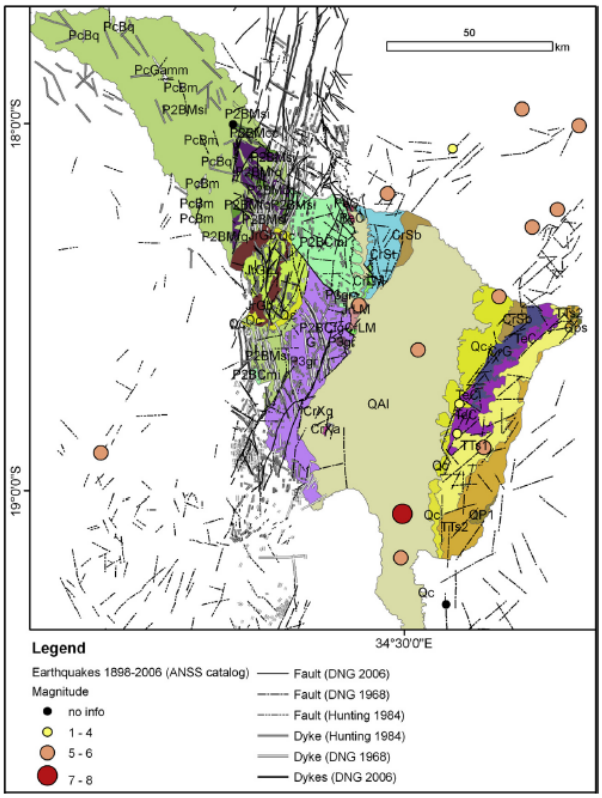

Fig. 39 Map of tectonic elements and seismic activities of the Gorongosa National Park (Steinbruch 2010).

According to the geological map, one can assume that sandstone may be found at varying depths throughout the area. Furthermore, the sandstone is of Cretaceous age while the gneiss is Precambrian. This indicates that sandstone was originally deposited on top of the gneiss, and the former should hence be represented in the profiles.

The stress map by Heidbach et al. (2008) suggest that the area is no longer tectonically active. This is, however, contradicted by Steinbruch (2010) (Fig. 39). The EARS rifting is related to the movement of the plate, caused by uplifting of the asthenosphere. Tectonic activity is characterized by earthquakes, and Urema Graben has frequent seismic activity at depths between 26 and 33 km and in magnitudes between 4 and 8 on the Richter scale (see Fig. 39). Field observations, as well as the local geological map, suggest the presence of several major faults in the area. The presence of these faults will most likely assist the surface water infiltration of the ground. Furthermore, an inferred infiltration zone is presumed present in the central unit (yellow), were numerous faults are found in the fractured gneiss. This will also contribute to the infiltration of deeper aquifers.

In addition, the grain size analysis of Area 1 support the interpretation of the resistivity profiles. All samples are of the medium to coarse sand fraction, except for one sample from the NW (sample 1_1c) and one from the SE (sample 1_1g) of LP1_1. Sample 1_1c mainly consist of gravelly sand, while sample 1_1g is comprised of almost pure medium sand. Unfortunately, it is not possible to observe variations in the sand fraction from the resistivity profiles.

Borehole 5 is unfortunately only represented by the first a 2.25 m, due to collapsing sidewalls, which made it impossible to drill any deeper. The result from the hand auger shows that Borehole 5 consists of silty to gravelly sand, which is to be expected according to the grain size analysis. This may be interpreted as resulting from surface erosion and variations in the water flow in the area. This correspond relatively well with the interpretations of the resistivity profiles.

Because of the high main percentage of mean residual, between 16 to 20.4%, in the IP profiles (Appendix 4), true interpretations based on these profiles are difficult to perform. All profiles contain some artifacts caused by noise in the data, but they are most distinguishable in LP1_1.

5.2 Area 2

All the three resistivity profiles from Area 2 (LP2_1, CPD2_2 and CPD 2_3; Fig. 40-42) are structured according to four identified units, the top red unit with high resistivity (330-1400 Ωm), the green unit with low resistivity (8.8-37 Ωm), the orange/yellow unit with medium resistivity (18-160 Ωm) and the bottom green unit with low resistivity (2.1-18 Ωm). Furthermore, the top unit of CPU2_2 also contain some areas with medium resistivity (37-160 Ωm). Like Area 1,

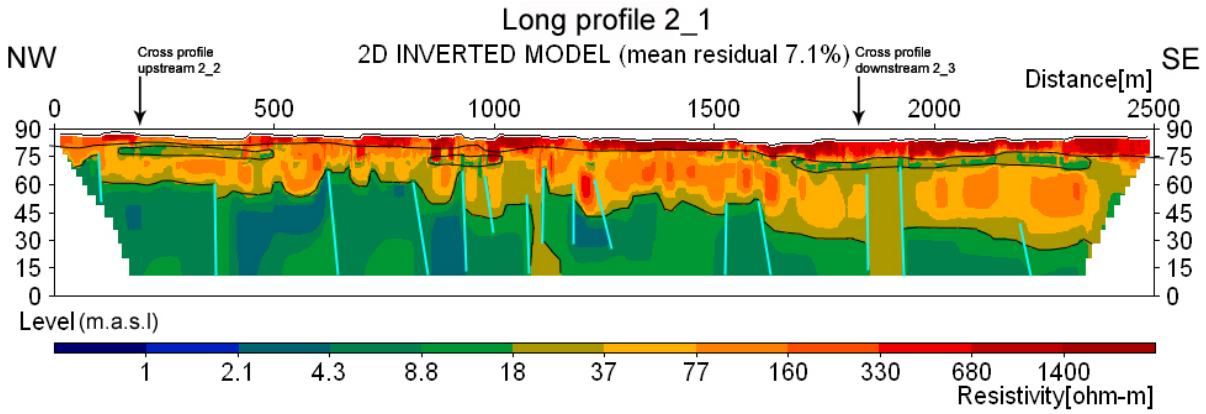

Fig. 40 Long profile 2_1 has a top unit consisting of sand, with silt/clay lenses. The bottom unit consist of sandstone. The blue lines represent possible faults.

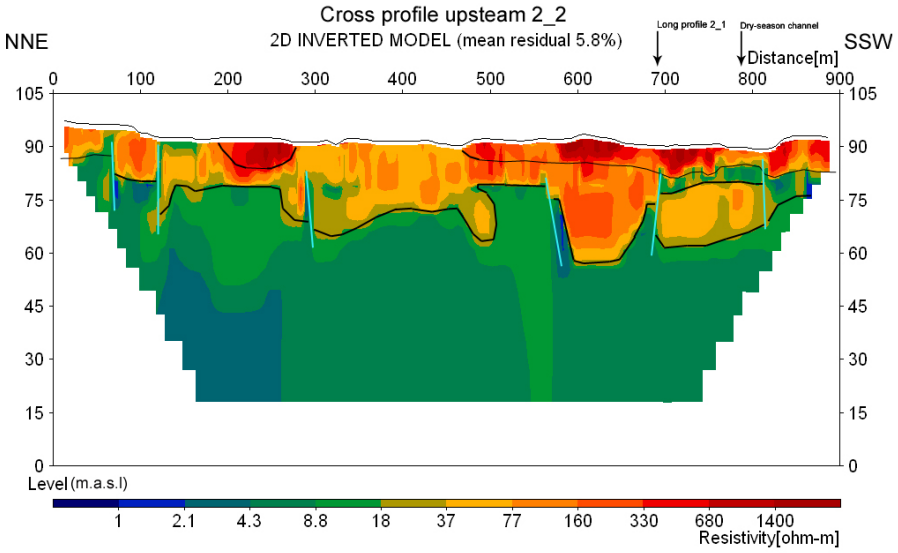

Fig. 41 Cross profile upstream 2_2 has a top unit consisting of sand, with silt/clay lenses. The bottom unit consist of sandstone. The blue lines represent possible faults.

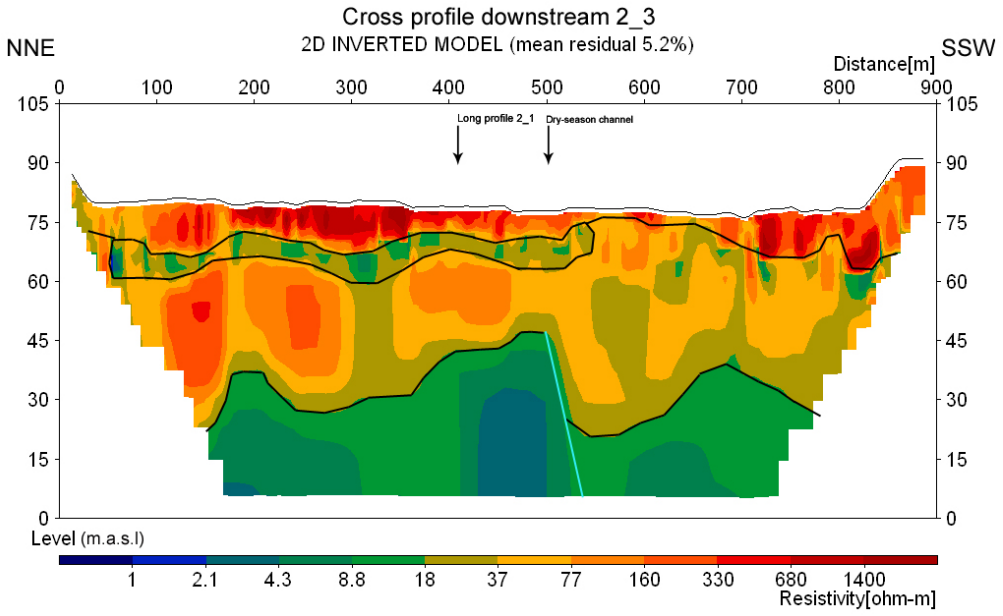

Fig. 42 Cross profile downstream 2_3 has a top unit consisting of sand, with silt/clay lenses. The bottom unit consist of sandstone. The blue lines represent possible faults.

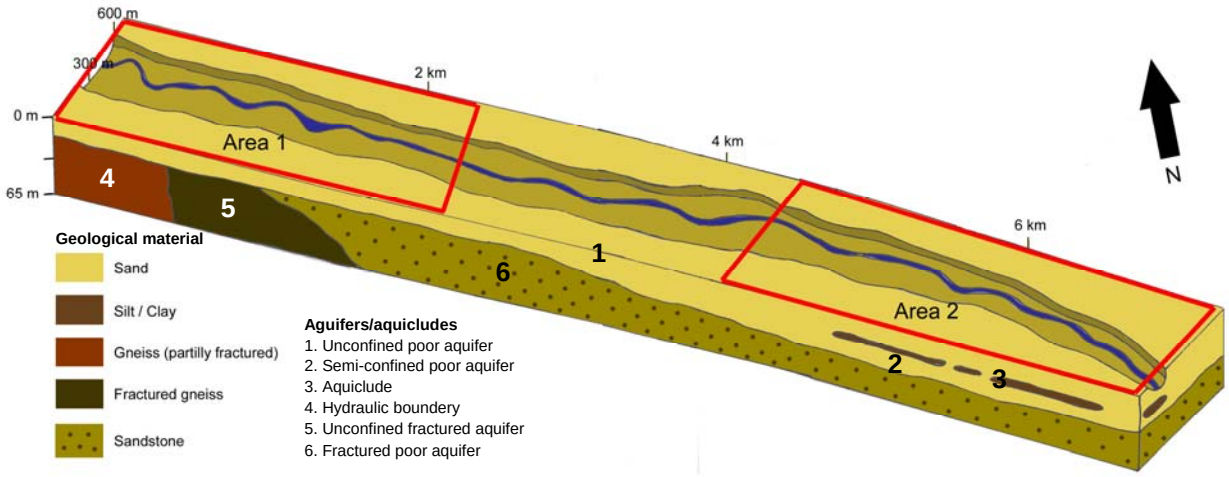

Fig. 43 Geological model over Area 1 and 2. Area 1 and 2 are marked by red rectangles. Five different units and aquifers/ aquicludes can be distinguished. The sand represent an unconfined poor aquifer (1) in the NW and a semi-confined aquifer (2) in the SE (below the silt/clay lenses), the silt/clay is classified as a aquiclude (3), the gneiss is a hydraulic boundary (4), the fractured gneiss is a unconfined fractured aquifer (5) and the sandstone is a fractured poor aquifer (6).

Area 2 contains numerous faults, identified as blue lines in the profiles.

The red unit in the profiles consist mainly of sand, as indicted by surface soil samples and augering. The sand changes from dry at the top to more saturated further down, while the sand is mixed with organic material on the river flanks, due to local vegetation. The second unit (green) consist of finer sediments, mainly silt and/or clay. The unit may be partially discontinuous, and, while visible in LP 2_1 and CPD2_3, it is more diffuse in CPU2_2. This has been interpreted as lenses (between 160 to 650 m long) of material, rather than being a continuous layer. This interpretation is quite plausible, since sediment lenses are not uncommon in faulted areas (Busby & Ingersoll 1995). It is, however, impossible to prove this hypothesis with the present data. The yellow unit is represented by a layer of saturated sand that thickens downstream (SE direction) according to the LP1_1 profile. This is also confirmed by both cross profiles, showing that the layer is only ~10-15 m thick upstream, while increasing to a thickness of ~40 m downstream. The dipping (SE direction) bottom unit (green) most likely represents the Sena sandstone and/ or Lupata sandstone, based on the two sedimentary rock samples that were collected (Appendix 1). The rock samples are terrigenous sandstones and have probably been deposit in a meandered river. Rock sample A has probably been deposited in the water at the deposition side, while Rock sample B has probably been deposit in higher water velocity on the erosion side. Furthermore, the weathered feldspar-rich sandstone found in situ has been altered in to kaolinite. However, it has also been suggested that the green bottom unit may consist mainly of finer sediment, primarily silt and/or clay (personal communication with R. Owen), but this can neither be proved nor disproved.

The interpretation of the topmost layer in the resistivity profiles has been verified by the grain size analyses of Area 2. All samples contain sand in different fractions from clayey silty sand to sandy gravel (Appendix 2). Borehole 4 and 6 only reach a shallow depth of 2.10 and 1.80 m, respectively, as a result of collapsing sidewalls making further drilling very difficult. The results from the hand auger show that the boreholes mainly consist of silty clayey sand to sand of the medium fraction. This may be interpreted as a result of surface erosion, in combination with variations in the water flow in the area.

The high main percentage of mean residual in the IP profiles, between 22 to 45.1%, make accurate and precise interpretations based on these profiles more difficult. CPD2_3 has the lowest error (22%) and the model is considered homogenous. The profile may represent sand or sandstone, since this geological material reveals no anomalies.

The normalized chargeability of CPD2_3 (Fig. 44) display elevated values in the NNE region of this profile. There is, however, a sudden dip present, which has been interpreted as a fault. This is corroborated by the results from the resistivity measurements (Fig. 42). Furthermore, the sandstone have probably varies in both composition and grain size, but these changes can only be observed to some degree in the normalized data.

5.3 Connecting Area 1 and 2

The difference between Area 1 and 2, according to the resistivity profiles, is the thickness and contents of the Quaternary sediments, as well as the frequency of bedrock (Fig. 43).

The resistivity profiles of Area 1 and 2 show that the two uppermost layers, consisting of sand and sandstone, are correlated to each other, but located at different depths. In Area 2 the Quaternary sediments

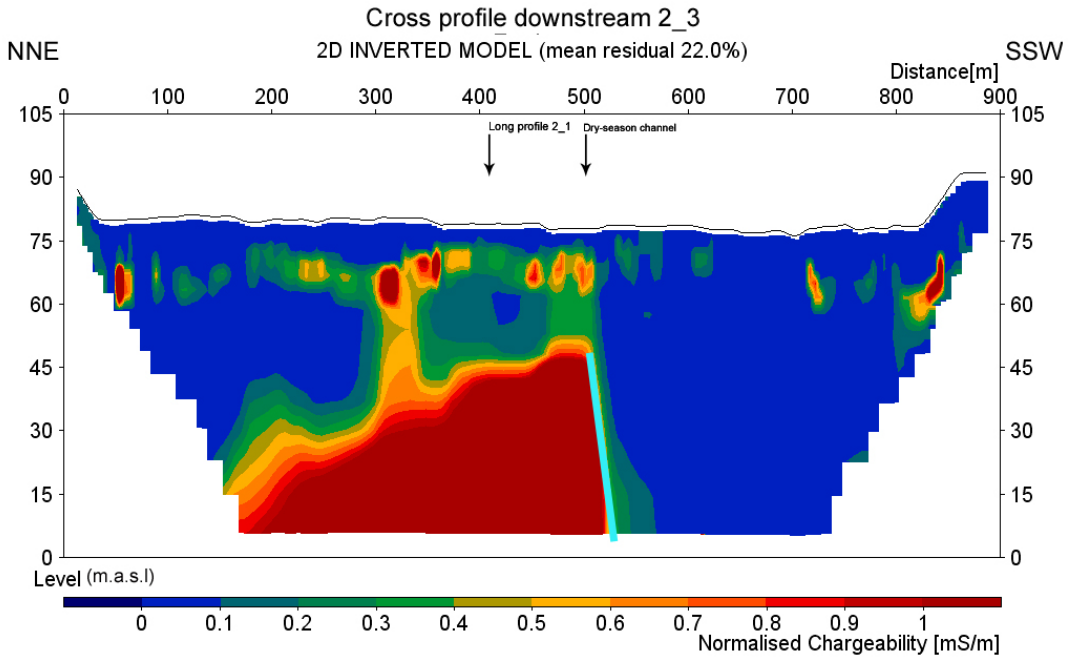

Fig. 44 Normalized chargeability of CPD2_3. The blue line represent possible fault.

include a layer of finer material (silt/clay) that is not present in Area 1. The lack of finer material may be explained by higher water velocity (> 1 cm/sec) in the area. In both Area 1 and 2, the Quaternary sediments are of terrigenous origin according to the carbonate content, and were deposited onto the bedrock by an alluvial process. These sediments are distributed evenly across Area 1, at a thickness of ~5-10 m. In Area 2 this layer increases in thickness downstream, from ~10-15 m in the NW to ~40 m in the SE. This wedge is probably caused by decreasing water velocity (< 10 cm/sec). Stronger water flow can transport larger particles and sediments (10 cm/sec for sand) further downstream, where the velocity decreases and sediments are finally deposited. In conclusion, the Quaternary sediments are getting thicker (~40 m) further downstream, and are expected to continue beyond Area 2 until we no longer can see the sandstone under the Quaternary sediments. The dip between the Quaternary sediments and the sandstone appears to be gradual, from ~6° in Area 1 to ~1.15° in Area 2, giving an average dip of ~0.69°/km toward the SE. This will result in a calculated depth of the sandstone below Lake Urema to approximately 2.8 km.

The maximum resistivity vary between Area 1 (3000 Ωm) and Area 2 (1400 Ωm), which is explained by differences in geological materials, and the related resistivity scale bars needed to give a good model. For example, solid gneiss generally has higher resistivity than finer sediments, such as silt and clay.

The mineralogy in Area 1 and 2 is quite similar. The major mineral groups found in both areas are crystalline bedrock, quartz and sandstone. Crystalline bedrock is present along the Nhandugue River in the north, and is possibly the source. The quartz and sandstone are derived from sandstone that is located south of the river, but the quartz may also be derived from erosion of the crystalline bedrock along the Nhandugue River. In addition, the surface sample from Area 2 contains a small number of volcanic particles and sedimentary concretions. According to the geological map, outcrops of phonolithic lava are present north of Area 2, and this could be a possible source for the volcanic material. No phonolithic lava has ever been associated with the Nhandugue River in Area 2. However, a contact has been located at the Muche River, which is a minor stream that connect to the Nhandugue River north of Area 2. Hence, it is most likely that this river supplies Area 2 with volcanic material from the NW. The origin of the secondary concretions are determine to decide due to the mixture of minerals, but probably originate from the gneiss.

5.4 Possible water reservoir?

The river discharge of Area 1 and 2 has been calculated to ~565 l/s and ~213 l/s, respectively, indicating that the discharge is more than twice as high in Area 1. A true discharge value can not be given for the main channel in Area 1, due to two major spikes observed in the diagram (see chapter 5.5). Still, the value appears reasonably and will be discussed further below. The difference observed in the discharges indicate an infiltration in the sediments, possibly by sinking water.

The discharge of Area 1 was collected on top of the outcrop, upstream of LP1_1 (Fig. 17). This means that there were no sediment on top of the gneiss and almost no infiltration, but some water may have infiltrated the fractures in the gneiss. Furthermore, the main flow occurred as surface water. The Quaternary sediments, and probably the sandstone, in both Area 1

and 2 are with high probability saturated. The uppermost sand layer in Area 1 and 2 is classified as a unconfined pore aquifer. The top ~5-10 m of Area 1 consists of a layer of sand that has the ability to transport significant quantities of water, and is classified as an aquifer (Fig. 43). In Area 2, the layer of sand are thicker (~10-15 m in the NW and ~40 m in the SE), but partly separated by silty/clayey lenses (between 160 to 650 m long). The sandy sediments are classified as an aquifer, and may be the same aquifer as in Area 1. The silty/clayey lenses have more moderate ability to transport quantities of water and hence is classified as an aqiclude.

The uppermost sand layer of Area 1 and 2 has a hydraulic conductivity of 10^{-4} to 10^{-3}m/s, which corresponds to Freeze & Cherry (1979) interpretation of geological material and hydraulic conductivity. According to Freeze & Cherry (1979), silty sand has a hydraulic conductivity of 10^{-7} to 10^{-3} m/s, while clean sand range between 10^{-6} and 10^{-2} m/s. From this information, the Quaternary sediments have been classified as a pore aquifer (Fig. 43). The aquifers in both areas have a hydraulic gradient to the SE, and has been classified as unconfined aquifers with direct contact to the atmosphere.

When a minor part of an unconfined aquifer is covered by an aquiclude, in this case at the SE part of the study area consisting of silty/clayey lenses, it may become a confined or semi-confined aquifer (depending on how you restrict an area). As a consequence of the thick Quaternary sediments present in Area 2, this area can transport higher volumes ground water in the studied cross-section. The solid gneiss form a hydraulic boundary, while the fractured gneiss is an unconfined fractured aquifer and a possible infiltration zone. The sandstone is here classified as a fractured pore aquifer. The quantity of water the sandstone may contain depends on the consolidation of the sediment. In the current setting, the sandstone is probably providing Lake Urema with water during the entire year, specifically through the fault located in the more narrow section of the river.

The river located in the survey area fluctuates between being a draining, neutral or a infiltrating river, all depending on current precipitation and the level of the ground water table.

The surface water of the river continuously infiltrates the ground water and probably affect the whole Urema Graben area. In conclusion, it is likely that Nhandugue River and other rivers in the area provide Lake Urema with water via the ground water, especially during dry season.

5.5 Sources of error

During resistivity and IP measurements occasionally negative resistivity readings occurred. This quality problem in measurements was caused by poor electrode contact, probably resulting from very dry sand surrounding the electrodes. The electrode contact was improved by cleaning the cable jumpers and contacts, as well as watering the ground with normal water and saltwater. If needed, several electrodes were also connected to the same electrode point. During the resistivity data process several bad data points were extracted to improve the data quality, but the mean residual percent is still high in some cases.

The very simple equipment used for the elevation survey also constituted an obvious source of error. The string between the metal sticks was somewhat elastic and hence difficult to extend to an identical length every time, particularly because of the vegetation. The reading of the hanging compass was problematic due to the weight not being fixed straight, which resulted in some subjectivity. After a while of use, the degree scale of the hanging compass was erased and new numbers had to be drawn on by hand. Furthermore, the metal sticks were supposed to be of the same height, at an angle of 90^{o}, but as some of the metal sticks became slightly bent, it became impossible to get the correct angle. Occasionally the soft ground also caused problems, since the sticks would sink slightly in the sand (~5-10 cm).

During the augering, no lining was used and the borehole kept filling in with sediment. This may have influenced the logging by contaminating the different layers. All soil samples that were collected in the field were reduced in size and weight, without using a sample divider. There is a minor risk that the splitting (by hand) has caused the samples to be slightly altered from the original size composition.

During the hydrometer analysis there was an error source during the first few seconds of the readings and the crushing of the sample. The hydrometer was bobbing and it was hard to read it correctly, but this step was repeated once to minimize the error. The samples used in the hydrometer analysis were crushed with a pestle. The result show a gap between the sieving and the hydrometer analysis, probably caused by the sample being crushed a little too much, and all larger fraction became slightly finer.

The discharge measurement of Area 1 was not accurate due to the loss of data from the third channel, as well as recording two spikes instead of one in the main channel. The loss of data from the third channel will probably not interfere with the interpretation, due to the small amount of water running in the channel. The two spikes were probably caused by either the NaCl tracer not being poured out properly as one unit, or the NaCl solution not being completely dissolved. Either case would result in readings with more concentrated NaCl present.

6 CONCLUSIONS

- The profiles show that the area has undergone some major tectonic processes in the past, and is presently active according to the seismic data. However, it is not possible to use the resistivity profiles to determine if the area is tectonically active.

- The carbonate content was identical in both areas (≤ 0.5%) which indicate a terrigenous origin. The mineralogy of Area 1 and 2 is quite similar, the three major types of bedrock are crystalline bedrock, quartz fragments and sandstone particles. The crystalline bedrock, and perhaps the quartz fragments, originate from gneiss in the NW, along the Nhandugue river. However, the quartz fragments can also originate from the sandstone located south of the river, as well as the sandstone particles.

  In Area 2, volcanic bedrock and secondary concretions are also present. The origin of the volcanic mineral is probably the phonolithic lava beds located north of the area, transported by the Muche river. The origin of the secondary concretions are more difficult, derive due to its complexity.

- The Quaternary sediments were deposited during alluvial processes and vary in thickness. In Area 1 the sediments are very shallow, between ~5-10 m thick. In the NW of Area 2, the Quaternary sediments are ~10-15 m thick, while they are ~40 m thick to the SE.

- One aquifer is located in Area 1, and two aquifers are located in Area 2. In both areas the aquifers are classified as unconfined pore aquifers, defined by the contact with the atmosphere, consisting of saturated sand. In addition, Area 2 has a semi-confined aquifer located under an aquiclude, consisting of silt/clay 160 to 650 m long lenses. The fractured gneiss is an unconfined fractured aquifer and the sandstone is a fractured pore aquifer. Due to the dip of the sandstone has the area a hydraulic gradient in a SE direction.

- Both gneiss and sandstone are located beneath the Quaternary sediments. The more solid gneiss in the NW of Area 1 form a hydraulic boundary with the fractured gneiss, which constitute a possible infiltration zone. The local sandstone probably represent the Sena Sandstone and/or the Lupata sandstone, and may interfere with the water flow to some extent. The sandstone is in all probability quite porous and saturated in water. The dip of the sandstone is a contributing factor to the hydraulic gradient.

- The surface water is infiltrating down to the ground water in the infiltration zone (fractured gneiss) in combination with the overlying sand. Hence, the ground water is probably infiltrating deeper aquifers, a process that is associated with the numerous faults that are present in the gneiss and sandstone.

7 RECOMMENDATIONS

To get additional information and deeper understanding of the ground water levels more studies are needed. More resistivity measurements downstream would provide additional information about possible aquifers or aquicludes. Aquicludes are more likely to be present downstream, due to the lower water velocity. To get a better picture of the drainage system to Lake Urema, resistivity measurements are needed north of Lake Urema, while possible recharge zones should be investigated by doing the same along the eastern rift margin.

An easy way to verify or disprove the hypothesis of the sandstone in this thesis would be to do resistivity measurements at the sandstone outcrop in Area 2. This would give information about the resistivity interval of the sandstone and clarity if the interpretation may be correct. If possible a cross profile through the valley would also yield much new information.

Supplementary annual discharge measurements would give a better picture of the recharge during a whole year, and if there is any differences between dry and wet season. Deeper boreholes that reach the sandstone at ~60 m, could provide important hydrological information about the changing ground water levels. During the drilling, soil sampling should be taken to confirm the resistivity profiles, while water sample can be collected for chemical analyses to establish the origin of the water. This will demonstrate if the infiltrated water also provide Lake Urema with water. To get a better overview of the hydraulic gradient, a number of deeper augering holes are also needed along the river.

8 ACKNOWLEDGEMENTS

I would like to give special tanks to:

- My supervisors Per Sandgren, University of Lund, and Torleif Dahlin, University of Lund, for all support during the fieldwork and writing this thesis.

- Richard Owen, University of Zimbabwe, for all feed back and help both in Mozambique and back home.

- Franziska Steinbruch for all help to organize the fieldwork and the feedback on the thesis. Also thanks for all help in Beira after the fieldwork.

- Farisse Chirindja, for being a big help in field and a link between the locals.

- Luigi Magaia and Felix Okeio, for great help in field.

- SIDA for the Minor Field Study scholarship and giving a good introductory course for working in developing countries.

- Elonio Muiuane, Eduardo Mondlane University, for providing transportation and equipment in field.

- Gorongosa National Park staff, for all help during the days in the camp.

- My family and friend, for always been there when I needed it. A special thanks to: Kristina Arvidsson for being a good travel companion to Mozambique and during the work of this thesis. Birgitta Stenberg, Per-Olof Stenberg and Anders Cronholm for all support during the thesis.

9 REFERENCES

ABEM, 2009: *Instruction Manual Terrameter SAS 4000 / SAS 1000*. ABEM Instrument AB, Sundbyberg, Sweden. 136 pp.

Ambrosiani, K.G., 1995: Kompendium i jordartsanalys - laboratorieanvisningar. *Quatrnaria Ser. B, 1*, 1-128.

Arvidsson, K., 2010: Geophysical and hydrogeological survey in a part of the Nhandugue river valley, Gorongosa National Park, Mozambique – Area 2 and 3. M.Sc thesis, Department of Earth and Ecosystem Sciences. *Examensarbete i geologi vid Lunds universitet 256*, 1-40.

Beilfuss, R., Steinbruch, F. & Owen, R., 2007: *Long termplan for hydrological research: adaptive management of water resources at Gorongosa National Park*. Report prepared for Gorongosa Research Center, Gorongosa National Park, Mozabique. 26 pp.

Busby, C. & Ingersoll, R., 1995: *Tectonics of Sedimentary Basins*. Malden. Blackwell Science 579 pp.

Böhme, B., 2005: Geo-ecology of lake Urema/central Mozambique. *Freiberg Online Geology, Freiberg, Germany 14*, 1-114.

Chirindja, F. & Hellman, K., 2009: Geophysical investtigation in a part of Gorongosa National Park in Mozambique – A Minor Field Study. M.Sc. thesis, Department of Engineering Geology, *Examensarbete i teknisk geologi vid Lunds universitet 1531*, 1-47.

Crossley, R., 1984: Controls of sedimentation in the Malawi rift valley, Central Africa. Zomba, Malawi. *Sedimentary geology 40*, 33-50.

Dahlin, T., 1993: *On the automation of 2D resistivity surveying for engineering and environmenta applications*. Ph.D. thesis, Department of Engineering Geology, Lund University, Lund, Sweden. 187 pp.

Dahlin, T., 2007: *Erigraph: user guide*. Lund, Sweden. 10 pp.

Dahlin, T. & Zhou, B., 2006: Multiple-gradient array measurements for multichannel 2D resistivity imaging. *Near Surface Geophysics 4*, 113-123.

Freeze, A. R. & Cherry, A. J., 1979: *Groundwater*. Englewood Cliffs, Prentice Hall. 604 pp.

Gorongosa National Park [GNP], 2009: (10 June 2010) http://www.gorongosa.net/.

Halkjaer, E., 2007: *Länder i fickformat 207 Mocambique/Malawi*. Utrikespolitiska Institutet, Stockholm, Sweden. 40 pp.

Jeppsson, H., 2004: *Geoelektriska metoder inom tillämpad geofysik*: *kompendium i Geofysiska undersökningsmetoder*. GEOC04 kursmaterial, Geologiska Institutionen, Lunds universitets, Lund, Sverige. 56 pp.

Leeder, M. R. & Gawthorpe, R. L., 1987: Sedimentary models for extensional tilt-block/half-graben basin. In: M.P. Coward, J.F. Dewey & P.L. Hancock (editors): Continental extensional tectonics. *Geological Society Special Publications 28*, 139-152.

Loke, M.H., 2004: *Tutorial: 2-D and 3-D electrical imaging surveys*. (24 Mars 2010) http://www.geoelectrical.com/downloads.php

Loke, M.H., 2009: *Tutorial: 2-D and 3-D electrical imaging surveys*. (24 May 2010) http://www.geoelectrical.com/downloads.php

Lächelt, S., 2004: *The geology and mineral resources of Mozambique*. National Directorate of Geology, Maputo, Mozambique. 515 pp.

National Directorate of Geology [DNG], 2006: *Geological map of Gorongosa, Mozambique. Scale 1:250 000*.

Owen, R., 2004: *The Millennium Ecosystem Assessment (MA): GM SAFMA Hydrogeology condition and trend report.* Mineral Resource Centre, University of Zimbabwe, Zimbabwe. 21pp.

Danish Institute For Human Rights, 2006: *Africa [map]* (11 Mars 2010) http://www.humanrights.dk.

Reynolds, J.M., 2006: *An introduction to applied and environmental geophysics*. 2 ed. Chichester. Wiley. 796 pp.

Sharma, P.V., 1986: *Geophysical methods in Geology*, Elsevier, New York. 422pp.

Slater, L. D. & Lesmes D., 2002: IP interpretation in environmental investigations. *Geophysics 6 7* , 77-88.

Steinbruch, F. & Merkel, B.J., 2008: Characterization of a Pleistocene thermal spring in Mozambique. *Hydrogeology Journal 16*, 1655-1668.

Steinbruch, F. & Vogler, L.: *Hydrochemical mapping of Springs on Mount Gorongosa in Central Mozambique*. (paper in preparation)

Steinbruch, F., 2010: Geology and geomorphology of Urema Graben with emphasis on the evolution of Lake Urema. *Journal of African Earth Sciences 58*, 272-284.

Tinley, K.L., 1977: *Framework of the Gorongosa ecosystem*. Ph.D. thesis, Faculty of Science, University of Pretoria, Pretoria. 184 pp.

Appendix 1

Geological map over Urema Graben filled with Quaternary sediment in the Gorongosa region at the scale 1:250 000. The west consist of the Báruè Platform and the east consist of the Cheringoma Platform. The study area is marked with the red rectangle.

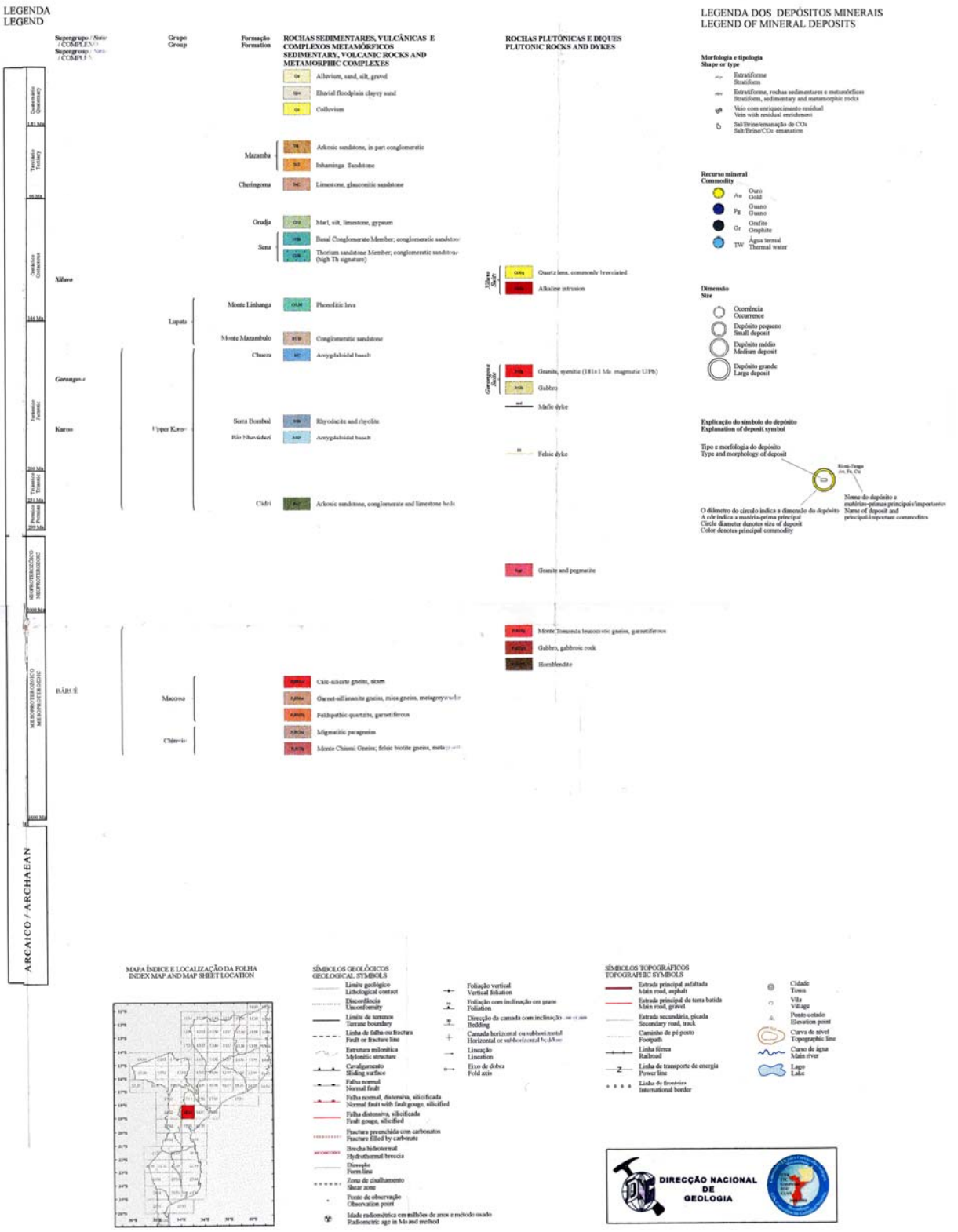
LEGENDA
LEGEND
Supergrupo / Super / COMPLEXO
Supergroup / Super / COMPLEX
Grupo
Group
Formação
Formation
ROCHAS SEDIMENTARES, VULCÂNICAS E COMPLEXOS METAMÓRFICOS SEDIMENTARY, VOLCANIC ROCKS AND METAMORPHIC COMPLEXES
Aluvião, areia, silte, cascalho
Aluvial floodplain clayey sand
Coluvião
Mazamba
Arkosic sandstone, in part conglomeratic
Inhaminga Sandstone
Cheringoma
Limestone, glauconitic sandstone
Grudja
Marl, silt, limestone, gypsum
Sena
Basal Conglomerate Member; conglomeratic sandstone
Thorium sandstone Member; conglomeratic sandstone (high Th signature)
Xiluvo
Lupata
Monte Linhanga
Phonolitic lava
Monte Mazambulo
Conglomeratic sandstone
Chuera
Amygdaloidal basalt
Karoo
Upper Karoo
Sena Bombué
Rhyodacite and rhyolite
Rio Nhavidzuri
Amygdaloidal basalt
Cidiri
Arkosic sandstone, conglomerate and limestone beds
BÁRUÉ
Macossa
Chimoio
Calc-silicate gneiss, skarn
Garnet-sillimanite gneiss, mica gneiss, metagreywacke
Feldspathic quartzite, garnetiferous
Migmatitic paragneiss
Monte Chissui Gneiss; felsic biotite gneiss, metagranite
ROCHAS PLUTÓNICAS E DIQUES
PLUTONIC ROCKS AND DYKES
Xiluvo Suite
Quartz lens, commonly brecciated
Alkaline intrusion
Gorongosa Suite
Granite, syenite (181±1 Ma magmatic U/Pb)
Gabbro
Mafic dyke
Felsic dyke
Granite and pegmatite
Monte Tomunda leucocratic gneiss, garnetiferous
Gabbro, gabbroic rock
Hornblendite
ARCAICO / ARCHAEAN
LEGENDA DOS DEPÓSITOS MINERAIS
LEGEND OF MINERAL DEPOSITS
Morfologia e tipologia
Shape or type
Estratiforme
Stratiform
Estratiforme, rochas sedimentares e metavulcânicas
Stratiform, sedimentary and metamorphic rocks
Veio com enriquecimento residual
Vein with residual enrichment
Sal/Brine/emanação de CO2
Salt/Brine/CO2 emanation
Recurso mineral
Commodity
Au Ouro
Gold
Pg Guano
Guano
Gr Grafite
Graphite
TW Água termal
Thermal water
Dimensão
Size
Ocorrência
Occurrence
Depósito pequeno
Small deposit
Depósito médio
Medium deposit
Depósito grande
Large deposit
Explicação do símbolo do depósito
Explanation of deposit symbol
Tipo e morfologia do depósito
Type and morphology of deposit
Nome do depósito e matérias-primas principais/importantes
Name of deposit and principal/important commodities
O diâmetro do círculo indica a dimensão do depósito
A cor indica a matéria-prima principal
Circle diameter denotes size of deposit
Color denotes principal commodity
MAPA ÍNDICE E LOCALIZAÇÃO DA FOLHA
INDEX MAP AND MAP SHEET LOCATION
SÍMBOLOS GEOLÓGICOS
GEOLOGICAL SYMBOLS
Limite geológico
Lithological contact
Discordância
Unconformity
Limite de terrenos
Terrane boundary
Linha de falha ou fractura
Fault or fracture line
Estrutura milonítica
Mylonitic structure
Cavalgamento
Sliding surface
Falha normal
Normal fault
Falha normal, distensiva, silicificada
Normal fault with fault gouge, silicified
Falha distensiva, silicificada
Fault gouge, silicified
Fractura preenchida com carbonatos
Fracture filled by carbonate
Brecha hidrotermal
Hydrothermal breccia
Direcção
Form line
Zona de cisalhamento
Shear zone
Ponto de observação
Observation point
Idade radiométrica em milhões de anos e método usado
Radiometric age in Ma and method
Foliação vertical
Vertical foliation
Foliação com inclinação em grau
Foliation
Direcção da camada com inclinação
Bedding
Camada horizontal ou subhorizontal
Horizontal or subhorizontal bedding
Lineação
Lineation
Eixo de dobra
Fold axis
SÍMBOLOS TOPOGRÁFICOS
TOPOGRAPHIC SYMBOLS
Estrada principal asfaltada
Main road, asphalt
Estrada principal de terra batida
Main road, gravel
Estrada secundária, picada
Secondary road, track
Caminho de pé posto
Footpath
Linha férrea
Railroad
Linha de transporte de energia
Power line
Linha de fronteira
International border
Cidade
Town
Vila
Village
Ponto cotado
Elevation point
Curva de nível
Topographic line
Curso de água
Main river
Lago
Lake
DIRECÇÃO NACIONAL DE GEOLOGIA

Appendix 2

Table of the grain size samples showing the percentage of each grain size and what the sample is classified as.

Area 1

Samples	Fraction (%)				Classification
	Gravel	Sand	Silt	Clay	
1_1a	0.94	98.91	0.15	0.00	Medium to coarse sand
1_1c	52.89	47.11	0.00	0.00	Sandy gravel
1_1e/1_2e	5.51	94.39	0.10	0.00	Medium to coarse sand
1_1g	1.48	97.63	0.89	0.00	Medium sand
1_3b	1.84	97.47	0.70	0.00	Medium to coarse sand
1_3c	6.17	93.19	0.64	0.00	Medium to coarse sand
BH5a	0.81	73.65	21.57	3.96	Silty sand
BH5b	2.70	70.71	9.10	17.49	Partly silty clayey sand
BH5c	10.73	83.54	5.73	0.00	Partly silty gravelly sand
BH5d	7.02	88.94	4.03	0.00	Coarse sand
BH5e	16.09	79.71	4.21	0.00	Gravelly sand

Area 2

Samples	Fraction (%)				Classification
	Gravel	Sand	Silt	Clay	
2_1b	28.37	71.24	0.39	0.00	Gravelly sand
2_1f	0.09	99.51	0.40	0.00	Medium sand
2_1g	0.19	77.48	13.80	8.53	Silty sand
2_2e	0.00	86.27	6.49	7.24	Fine sand
2_3a	0.15	68.84	20.42	10.59	Clayey silty sand
2_3b	1.39	93.35	5.26	0.00	Medium sand
2_3c	49.56	47.98	2.47	0.00	Sandy gravel
2_3d	6.23	87.49	6.29	0.00	Medium to coarse sand
Gravel Pit	37.90	45.28	2.09	14.73	Clayey gravelly sand
BH4a	1.20	48.77	15.18	34.86	Silty clayey sand
BH4b	6.93	52.57	13.96	26.54	Silty clayey sand
BH4c	2.26	51.07	16.94	29.72	Silty clayey sand
BH4d	1.11	65.65	11.32	21.92	Silty clayey sand
BH4e	9.09	78.21	4.58	8.13	Silty sand
BH4f	16.48	75.74	7.78	0.00	Medium to coarse sand
BH4g	8.82	81.48	4.31	5.38	Clayey sand
BH4h	30.09	64.69	5.22	0.00	Silty grvelly sand
BH6a	0.45	55.46	28.85	15.24	Clayey silty sand
BH6b	0.51	88.88	5.29	5.32	Partly silty clayey sand
BH6c	3.05	91.79	5.16	0.00	Partly silty sand
BH6d	0.30	96.03	3.67	0.00	Medium to coarse sand
BH6e	9.89	84.92	5.19	0.00	Partly silty sand

Appendix 3

Resistivity models from Area 1. (a) Long profile 1_1 (b) Cross profile Upstream 1_2, (c) Cross profile downstream 1_3.

a)

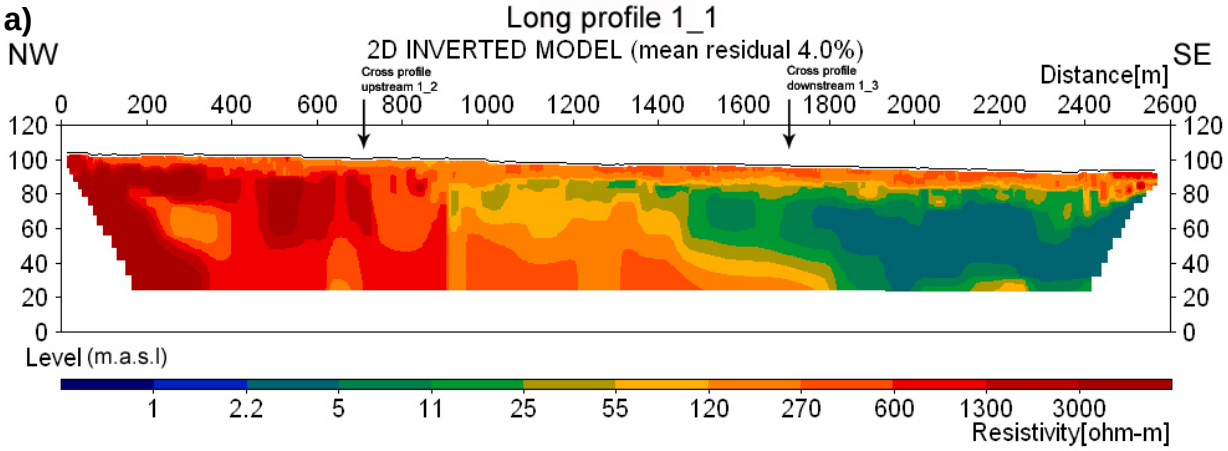

b)

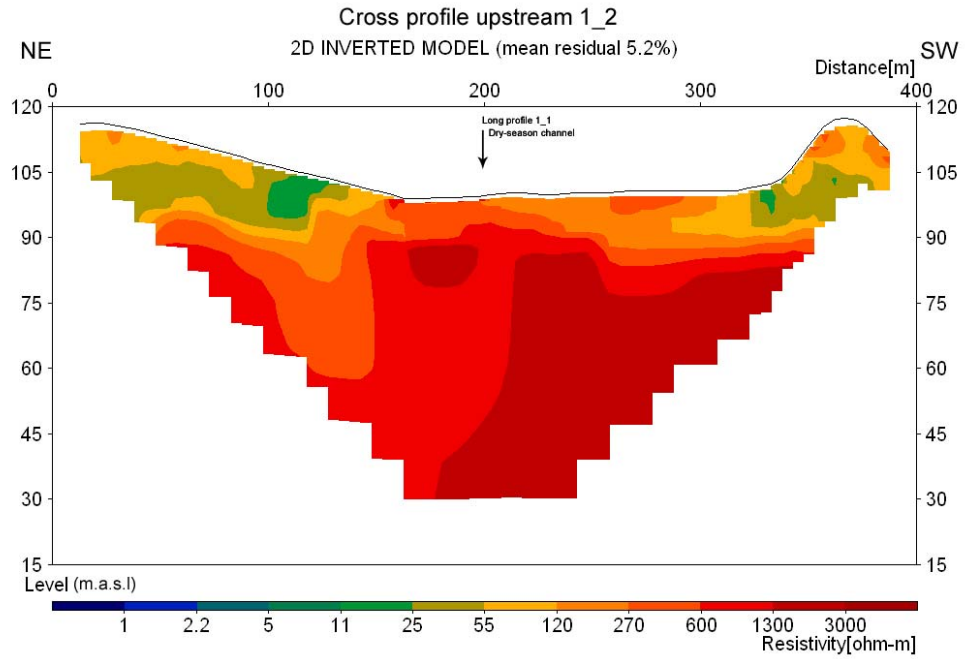

c)

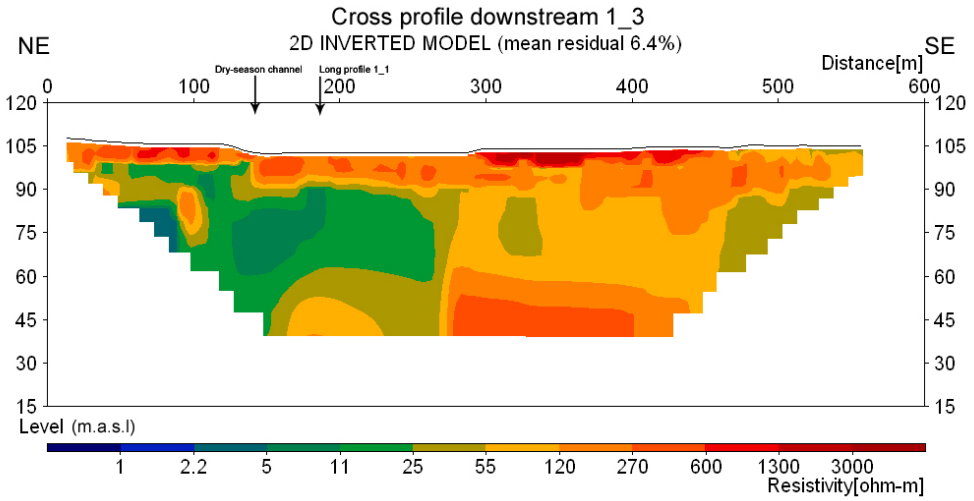

Appendix 4

IP models from Area 1. (a) Long profile 1_1 (b) Cross profile Upstream 1_2, (c) Cross profile downstream 1_3.

a)

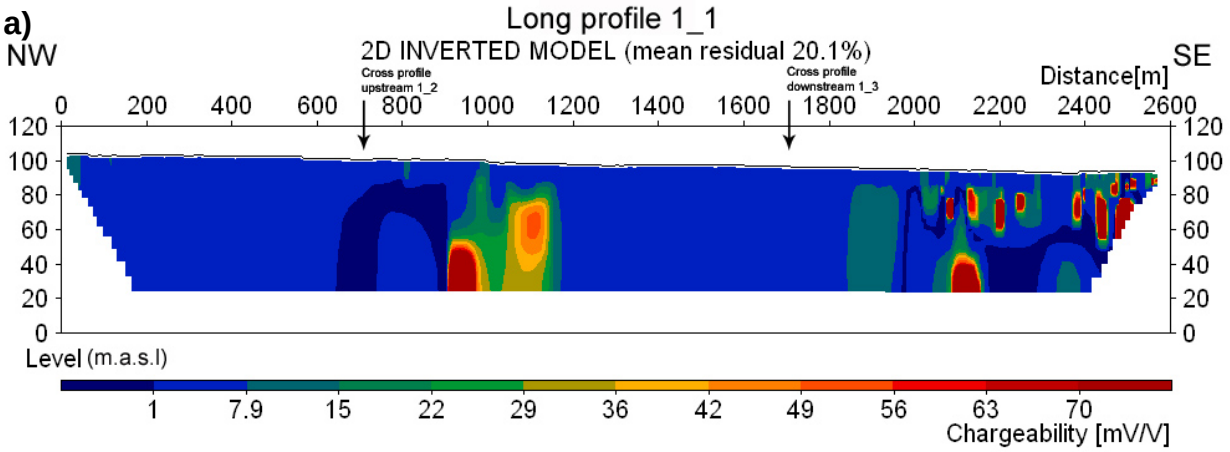

b)

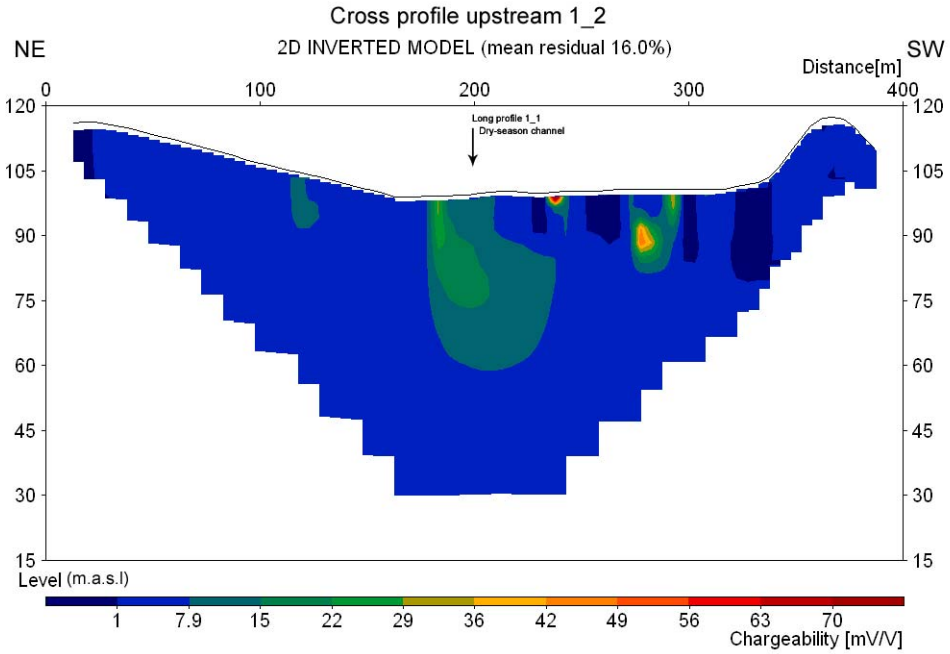

c)

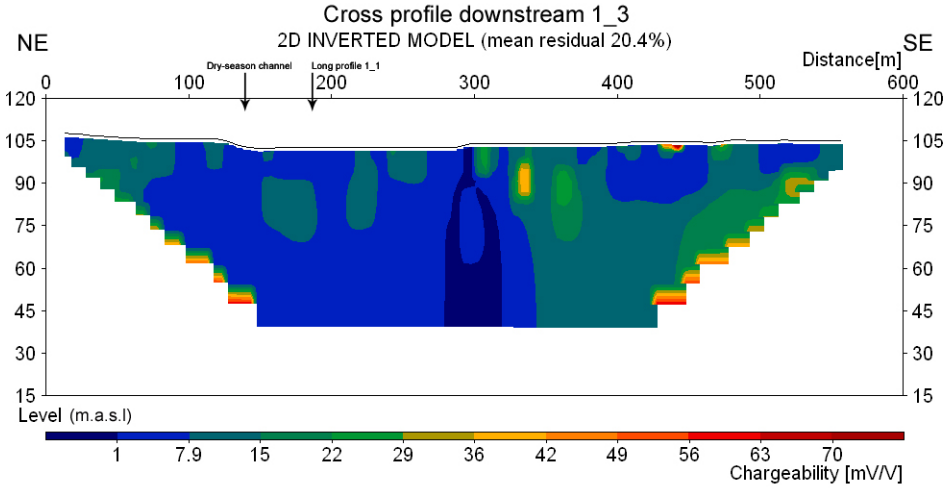

Appendix 5

Resistivity models from Area 2. (a) Long profile 2_1 (b) Cross profile Upstream 2_2, (c) Cross profile downstream 2_3.

a)

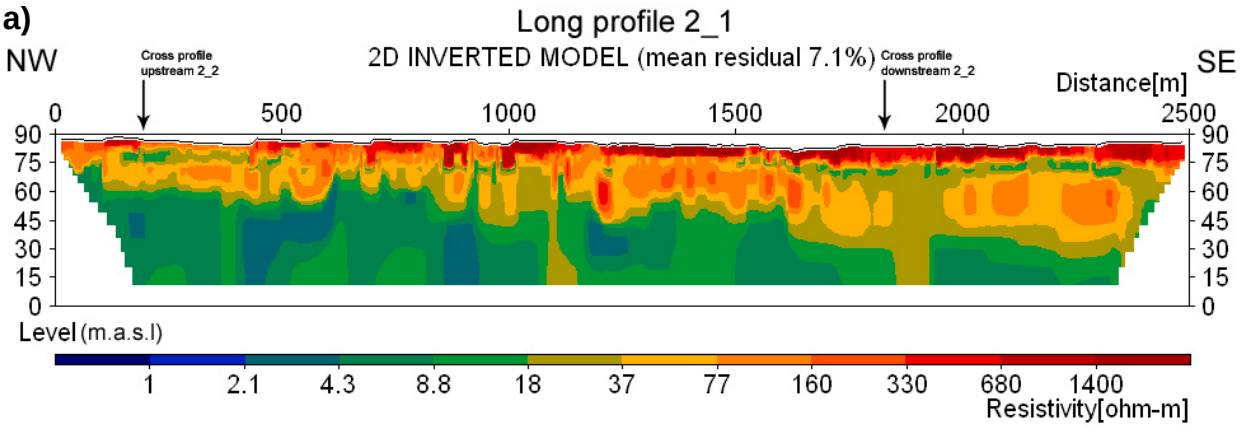

b)

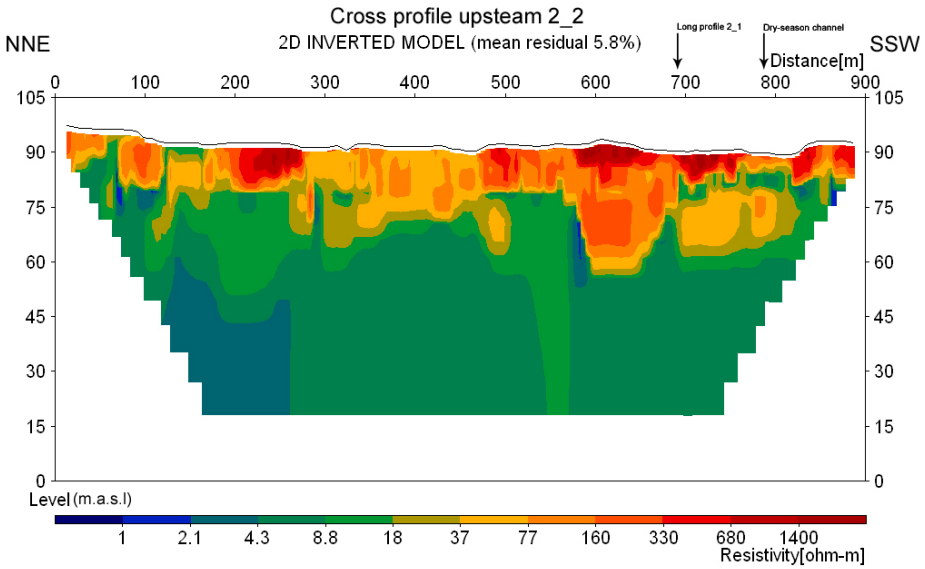

c)

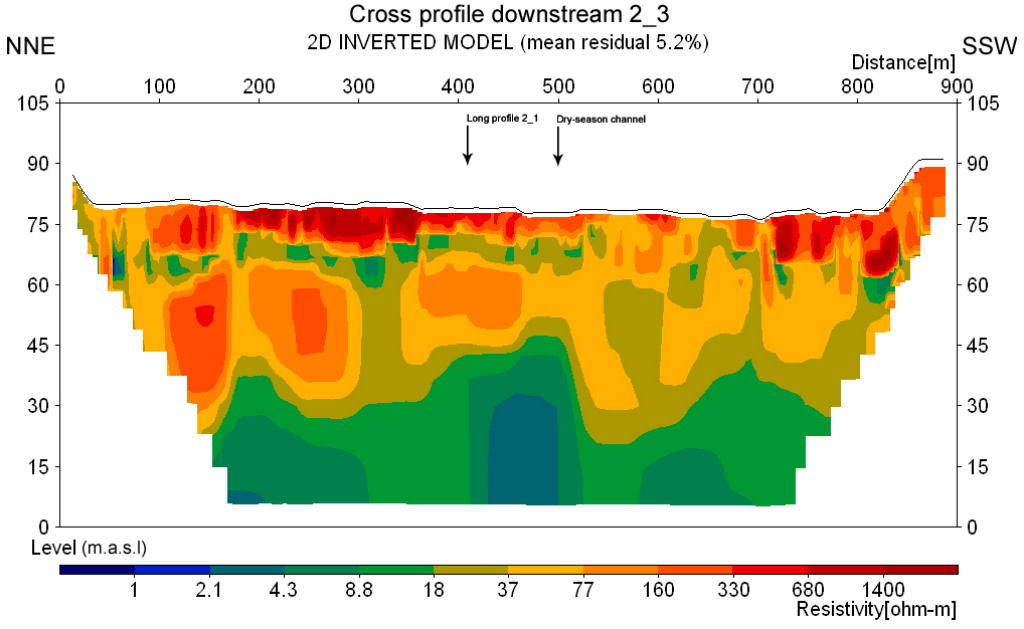

Appendix 6

IP models from Area 2. (a) Long profile 2_1 (b) Cross profile Upstream 2_2, (c) Cross profile downstream 2_3.

a)

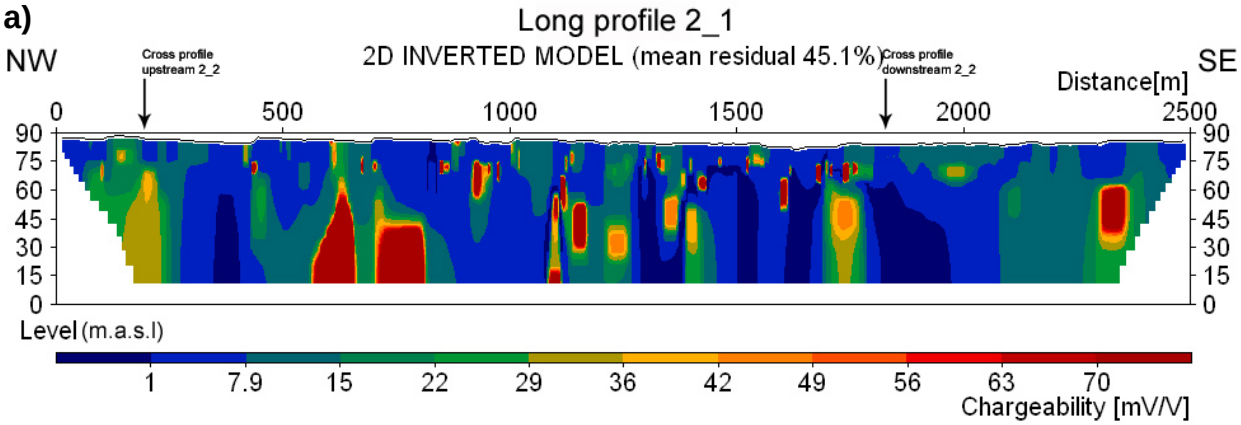

b)

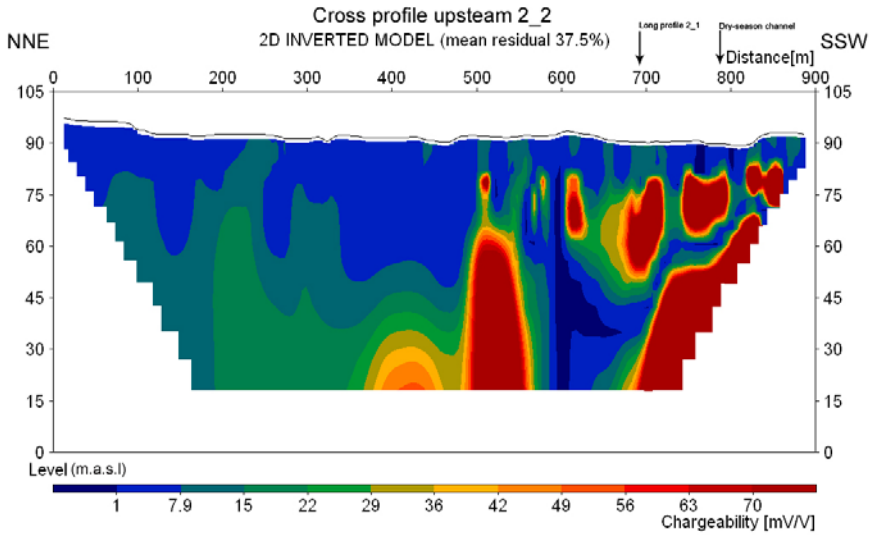

c)

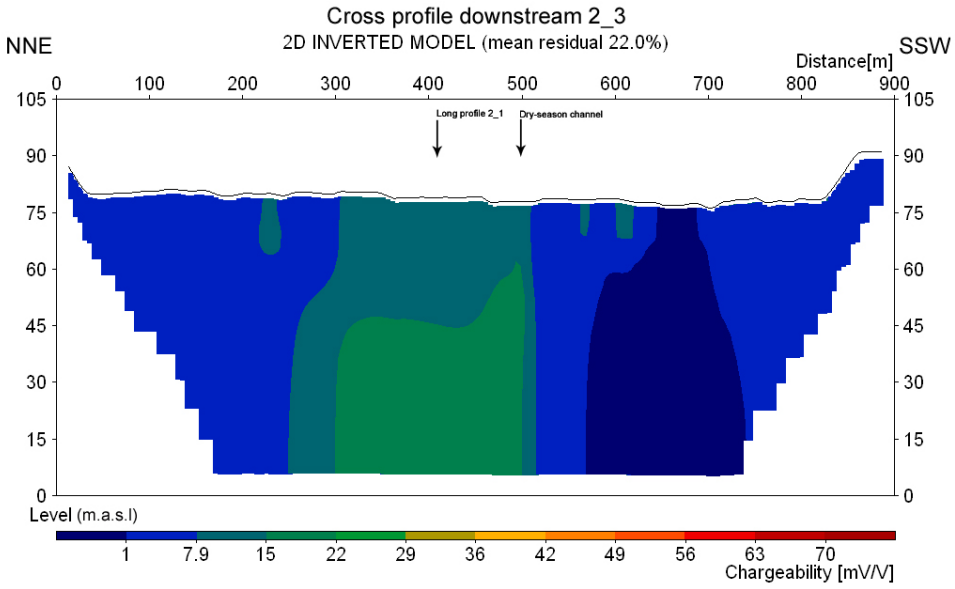

Tidigare skrifter i serien ”Examensarbeten i Geologi vid Lunds Universitet”:

216. Trondman, Anna-Kari, 2007: Stratigraphic studies of a Holocene sequence from Taniente Palet bog, Isla de los Estados, South America.
217. Månsson, Carl-Henrik & Siikanen, Jonas, 2007: Measuring techniques of Induced Polarization regarding data quality with an application on a test-site in Aarhus, Denmark and the tunnel construction at the Hallandsås Horst, Sweden.
218. Ohlsson, Erika, 2007: Classification of stony meteorites from north-west Africa and the Dhofar desert region in Oman.
219. Åkesson, Maria, 2008: Mud volcanoes - a review. (15 hskp)
220. Randsalu, Linda, 2008: Holocene relative sea-level changes in the Tasiusaq area, southern Greenland, with focus on the Ta1 and Ta3 basins. (30 hskp)
221. Fredh, Daniel, 2008: Holocene relative sea-level changes in the Tasiusaq area, southern Greenland, with focus on the Ta4 basin. (30 hskp)
222. Anjar, Johanna, 2008: A sedimentological and stratigraphical study of Weichselian sediments in the Tvärkroken gravel pit, Idre, west-central Sweden. (30 hskp)
223. Stefanowicz, Sissa, 2008: Palyno-stratigraphy and palaeoclimatic analysis of the Lower - Middle Jurassic (Pliens-bachian - Bathonian) of the Inner Hebrides, NW Scotland. (15 hskp)
224. Holm, Sanna, 2008: Variations in impactor flux to the Moon and Earth after 3.85 Ga. (15 hskp)
225. Bjärnborg, Karolina, 2008: Internal structures in detrital zircons from Hamrånge: a study of cathodolumine-scence and back-scattered electron images. (15 hskp)
226. Noresten, Barbro, 2008: A reconstruction of subglacial processes based on a classification of erosional forms at Ramsvikslandet, SW Sweden. (30 hskp)
227. Mehlqvist, Kristina, 2008: En mellanjuras-sisk flora från Bagå-formationen, Bornholm. (15 hskp)
228. Lindvall, Hanna, 2008: Kortvariga effekter av tefranedfall i lakustrin och terrestrisk miljö. (15 hskp)
229. Löfroth, Elin, 2008: Are solar activity and cosmic rays important factors behind climate change? (15 hskp)
230. Damberg, Lisa, 2008: Pyrit som källa för spårämnen – kalkstenar från övre och mellersta Danien, Skåne. (15 hskp)
331. Cegrell, Miriam & Mårtensson, Jimmy, 2008: Resistivity and IP measurements at the Bolmen Tunnel and Ådalsbanan, Sweden. (30 hskp)
232. Vang, Ina, 2008: Skarn minerals and geological structures at Kalkheia, Kristiansand, southern Norway. (15 hskp)
233. Arvidsson, Kristina, 2008: Vegetationen i Skandinavien under Eem och Weichsel samt fallstudie i submoräna organiska avlagringar från Nybygget, Småland. (15 hskp)
234. Persson, Jonas, 2008: An environmental magnetic study of a marine sediment core from Disko Bugt, West Greenland: implications for ocean current variability. (30 hskp)
235. Holm, Sanna, 2008: Titanium- and chromium-rich opaque minerals in condensed sediments: chondritic, lunar and terrestrial origins. (30 hskp)
236. Bohlin, Erik & Landen, Ludvig, 2008: Geofysiska mätmetoder för prospektering till ballastmaterial. (30 hskp)
237. Brodén, Olof, 2008: Primär och sekundär migration av hydrokarboner. (15 hskp)
238. Bergman, Bo, 2009: Geofysiska analyser (stångslingram, CVES och IP) av lagerföljd och lakvattenrörelser vid Albäcksdeponin, Trelleborg. (30 hskp)
239. Mehlqvist, Kristina, 2009: The spore record of early land plants from upper Silurian strata in Klinta 1 well, Skåne, Sweden. (45 hskp)
239. Mehlqvist, Kristina, 2009: The spore record of early land plants from upper Silurian strata in Klinta 1 well, Skåne, Sweden. (45 hskp)
240. Bjärnborg, Karolina, 2009: The copper sulphide mineralization of the Zinkgruvan deposit, Bergslagen, Sweden. (45 hskp)
241. Stenberg, Li, 2009: Historiska kartor som hjälp vid jordartsgeologisk kartering – en pilotstudie från Vångs by i Blekinge. (15 hskp)
242. Nilsson, Mimmi, 2009: Robust U-Pb

baddeleyite ages of mafic dykes and intrusions in southern West Greenland: constraints on the coherency of crustal blocks of the North Atlantic Craton. (30 hskp)

243. Hult, Elin, 2009: Oligocene to middle Miocene sediments from ODP leg 159, site 959 offshore Ivory Coast, equatorial West Africa. (15 hskp)
244. Olsson, Håkan, 2009: Climate archives and the Late Ordovician Boda Event. (15 hskp)
245. Wollein Waldetoft, Kristofer, 2009: Svekofennisk granit från olika metamorfa miljöer. (15 hskp)
246. Månsby, Urban, 2009: Late Cretaceous coprolites from the Kristianstad Basin, southern Sweden. (15 hskp)
247. MacGimpsey, I., 2008: Petroleum Geology of the Barents Sea. (15 hskp)
248. Jäckel, O., 2009: Comparison between two sediment X-ray Fluorescence records of the Late Holocene from Disko Bugt, West Greenland; Paleoclimatic and methodological implications. (45 hskp)
249. Andersen, Christine, 2009: The mineral composition of the Burkland Cu-sulphide deposit at Zinkgruvan, Sweden – a supplementary study. (15 hskp)
250. Riebe, My, 2009: Spinel group minerals in carbonaceous and ordinary chondrites. (15 hskp)
251. Nilsson, Filip, 2009: Föroreningsspridning och geologi vid Filborna i Helsingborg. (30 hskp)
252. Peetz, Romina, 2009: A geochemical characterization of the lower part of the Miocene shield-building lavas on Gran Canaria. (45 hskp)
253. Åkesson, Maria, 2010: Mass movements as contamination carriers in surface water systems – Swedish experiences and risks.
254. Löfroth, Elin, 2010: A Greenland ice core perspective on the dating of the Late Bronze Age Santorini eruption. (45 hskp)
255. Ellingsgaard, Óluva, 2009: Formation Evaluation of Interlava Volcaniclastic Rocks from the Faroe Islands and the Faroe-Shetland Basin. (45 hskp)
256. Arvidsson, Kristina, 2010: Geophysical and hydrogeological survey in a part of the Nhandugue River valley, Gorongosa National Park, Mozambique. (45 hskp)
257. Gren, Johan, 2010: Osteo-histology of Mesozoic marine tetrapods – implications for longevity, growth strategies and growth rates. (15 hskp)
258. Syversen, Fredrikke, 2010: Late Jurassic deposits in the Troll field. (15 hskp)
259. Andersson, Pontus, 2010: Hydrogeological investigation for the PEGASUS project, southern Skåne, Sweden. (30 hskp)
260. Noor, Amir, 2010: Upper Ordovician through lowermost Silurian stratigraphy and facies of the Borenshult-1 core, Östergötland, Sweden. (45 hskp)
261. Lewerentz, Alexander, 2010: On the occurrence of baddeleyite in zircon in silica-saturated rocks. (15 hskp)
262. Eriksson, Magnus, 2010: The Ordovician Orthoceratite Limestone and the Blommiga Bladet hardground complex at Horns Udde, Öland. (15 hskp)
263. Lindskog, Anders, 2010: From red to grey and back again: A detailed study of the lower Kundan (Middle Ordovician) 'Täljsten' interval and its enclosing strata in Västergötland, Sweden. (15 hskp)
264. Rääf, Rebecka, 2010: Changes in beyrichiid ostracode faunas during the Late Silurian Lau Event on Gotland, Sweden. (30 hskp)
265. Petersson, Andreas, 2010: Zircon U-Pb, Hf and O isotope constraints on the growth versus recycling of continental crust in the Grenville orogen, Ohio, USA. (45 hskp)
266. Stenberg, Li, 2010: Geophysical and hydrogeological survey in a part of the Nhandugue River valley, Gorongosa National Park, Mozambique – Area 1 and 2. (45 hskp)

LUNDS UNIVERSITET

Geologiska enheten
Institutionen för geo- och ekosystemvetenskaper
Sölvegatan 12, 223 62 Lund